

*Communications in
Applied
Mathematics and
Computational
Science*

SECOND-ORDER ACCURACY OF
VOLUME-OF-FLUID INTERFACE
RECONSTRUCTION ALGORITHMS
II: AN IMPROVED CONSTRAINT ON THE CELL
SIZE

ELBRIDGE GERRY PUCKETT

vol. 8 no. 1 2013

SECOND-ORDER ACCURACY OF VOLUME-OF-FLUID INTERFACE RECONSTRUCTION ALGORITHMS II: AN IMPROVED CONSTRAINT ON THE CELL SIZE

ELBRIDGE GERRY PUCKETT

In a previous article in this journal the author proved that, given a square grid of side h covering a two times continuously differentiable simple closed curve z in the plane, one can construct a pointwise second-order accurate piecewise linear approximation \tilde{z} to z from just the volume fractions due to z in the grid cells. In the present article the author proves a sufficient condition for \tilde{z} to be a second-order accurate approximation to z in the max norm is h must be bounded above by $2/(33\kappa_{\max})$, where κ_{\max} is the maximum magnitude of the curvature κ of z . This constraint on h is solely in terms of an intrinsic property of the curve z , namely κ_{\max} , which is invariant under rotations and translations of the grid. It is also far less restrictive than the constraint presented in the previous article. An important consequence of the proof in the present article is that the max norm of the difference $z - \tilde{z}$ depends linearly on κ_{\max} .

1. Introduction

The topic of this article is the *interface reconstruction problem* for a volume-of-fluid method in two space dimensions. This problem can be described as follows. Let $\Omega \subset \mathbb{R}^2$ denote a closed and bounded rectangular region in the plane, and let Ω_1 and Ω_2 be disjoint, connected (but not necessary simply connected) relatively open regions such that $\overline{\Omega}_1 \cup \overline{\Omega}_2 = \Omega$ and that $\overline{\Omega}_1 \cap \overline{\Omega}_2$ is the image of a twice continuously differentiable simple closed curve in Ω , denoted by $z(s) = (x(s), y(s))$, where s is arc length. The regions Ω_1 and Ω_2 contain “material 1” and “material 2”, respectively, where each material may be a thought of as a gas, fluid or solid and z is the boundary or *interface* between these two materials.

Let L be a characteristic length of the problem domain Ω and cover Ω with a grid Ω^h consisting of square cells, each of side $h \ll L$. Given integers i and j ,

Sponsored by the US Department of Energy Mathematical, Information, and Computing Sciences Division contracts DE-FC02-01ER25473 and DE-FG02-03ER25579.

MSC2010: primary 65M12, 76T99; secondary 65M06, 76M12, 76M25.

Keywords: volume-of-fluid, piecewise linear interface reconstruction, fronts, front reconstruction, interface reconstruction, two-phase flow, multiphase systems, under-resolved computations, computational fluid dynamics.

let $x_i = ih$ (resp. $y_j = jh$) denote the location of the i -th vertical (resp. j -th horizontal) grid line and let (x_i, y_j) denote the lower left hand corner of the ij -th cell

$$C_{ij} \stackrel{\text{def}}{=} [x_i, x_{i+1}] \times [y_j, y_{j+1}] \quad (1)$$

in the grid.

Denote the fraction of material 1 in the ij -th cell by Λ_{ij} . For each i, j the number Λ_{ij} satisfies $0 \leq \Lambda_{ij} \leq 1$ and is called the *volume fraction* (of material 1) in the ij -th cell. (Even though in two dimensions Λ_{ij} is technically an *area* fraction, the convention is to refer to it as a volume fraction.) Thus $0 < \Lambda_{ij} < 1$ if and only if a portion of the interface $\mathbf{z}(s)$ lies in the ij -th cell and $\Lambda_{ij} = 1$ (resp. $\Lambda_{ij} = 0$) if and only if the ij -th cell contains only material 1 (resp. material 2). In the volume-of-fluid interface reconstruction problem one is asked to determine an approximation $\tilde{\mathbf{z}}(s)$ to $\mathbf{z}(s)$ in Ω given only the volume fractions Λ_{ij} .

Suppose the interface $\mathbf{z}(s)$ passes through the ij -th cell C_{ij} and can be written as a single-valued function of x in C_{ij} ; that is, for $x \in [x_i, x_{i+1}]$ the interface can be written in the form $\mathbf{z}(s) = (x(s), y(s)) = (x(s), g(x(s)))$. Let $\tilde{g}_{ij}(x)$ denote an approximation to the interface in C_{ij} . Then the max norm of the difference between the interface $(x, g(x))$ and the approximate interface $(x, \tilde{g}_{ij}(x))$ in C_{ij} is defined in the usual way,

$$\|g - \tilde{g}_{ij}\|_{\infty(ij)} \stackrel{\text{def}}{=} \max_{x \in [x_i, x_{i+1}]} |g(x) - \tilde{g}_{ij}(x)|. \quad (2)$$

In the event the interface in the ij -th cell can only be expressed as a single-valued function $G(y)$ of $y \in [y_j, y_{j+1}]$ the max norm of the difference between the interface $(G(y), y)$ and the approximate interface $(\tilde{G}_{ij}(y), y)$ is defined analogously.

By [Theorem A.1](#) in the [Appendix](#), if the interface $\mathbf{z}(s) \in C^2(\mathbb{R})$ passes through the ij -th cell C_{ij} and the constraint in [\(5\)–\(6\)](#) below is satisfied, then it is possible to represent $\mathbf{z}(s)$ as either a single-valued function $y = g(x)$ or $x = G(y)$ of the independent variable x (resp. y) in the 3×3 block of cells B_{ij} centered on C_{ij} . For convenience, in all of the following the interface is assumed to be of the form $y = g(x)$ in the block B_{ij} with material 1 lying *below* the graph of g in B_{ij} ; it being understood that all of the definitions, results, etc. in this article also apply to the case in which the interface can only be expressed as a single-valued function $x = G(y)$ in B_{ij} . In [Section 2.1](#) I will present an algorithm for determining which of the four standard rotations of B_{ij} about its center, 0, 90, 180, or 270 degrees, will orient the block B_{ij} so the interface can be expressed as either $y = g(x)$ or $x = G(y)$ with material 1 lying below the interface.

Let $\kappa(s)$ denote the curvature of the interface $\mathbf{z}(s)$ and let

$$\kappa_{\max} \stackrel{\text{def}}{=} \max_s |\kappa(s)| \quad (3)$$

denote the maximum of the magnitude of $\kappa(s)$ in Ω . The main result of this article is as follows. If conditions (I)–(V) below hold, then the piecewise linear volume-of-fluid approximation $\tilde{g}_{ij}(x)$ defined in equations (7)–(10) below will approximate the true interface $z(s) = (x(s), g(x(s)))$ to second-order in h in the max norm,

$$\|g - \tilde{g}_{ij}\|_{\infty(ij)} \leq C_m \kappa_{\max} h^2 \quad \text{for all } i, j \text{ such that } 0 < \Lambda_{ij} < 1, \quad (4)$$

where the constant C_m , defined in (59) below, is independent of h and κ_{\max} . Note the linear dependence of the bound in (4) on κ_{\max} .

The following conditions are sufficient to ensure that (4) holds. Note that (II)–(IV) constitute an algorithm for constructing the piecewise linear approximation \tilde{z} to z . This algorithm is described in detail in [24].

(I) The interface $z = (x(s), y(s))$ is a two times continuously differentiable simple closed curve in Ω .

(II) The grid size h and the maximum magnitude κ_{\max} of the curvature of the interface satisfy the following inequality with respect to one another,

$$h \leq \frac{C_h}{\kappa_{\max}}, \quad (5)$$

where

$$C_h \stackrel{\text{def}}{=} \frac{2}{33}. \quad (6)$$

(III) In each cell C_{ij} that contains a portion of the interface $(x, g(x))$ the piecewise linear approximation

$$\tilde{g}_{ij}(x) \stackrel{\text{def}}{=} m_{ij}x + b_{ij} \quad (7)$$

to g in C_{ij} has the same volume fraction $\Lambda_{ij}(\tilde{g})$ in C_{ij} as does the interface,

$$\Lambda_{ij}(\tilde{g}) = \Lambda_{ij}(g). \quad (8)$$

See Figure 1 for an example. Note that, once the slope m_{ij} in (7) is given, the constraint in (8) uniquely determines b_{ij} .

(IV) In each cell C_{ij} that contains a portion of the interface, the slope m_{ij} of the piecewise linear approximation $\tilde{g}_{ij}(x)$ defined in (7) is given by

$$m_{ij} \stackrel{\text{def}}{=} \frac{S_{i+\alpha} - S_{i+\beta}}{\alpha - \beta} \quad \text{for some } \alpha, \beta = -1, 0, 1 \text{ with } \alpha \neq \beta, \quad (9)$$

where

$$S_{i+\alpha} \stackrel{\text{def}}{=} \sum_{j'=j-1}^{j+1} \Lambda_{i+\alpha, j'} \quad \text{and} \quad S_{i+\beta} \stackrel{\text{def}}{=} \sum_{j'=j-1}^{j+1} \Lambda_{i+\beta, j'} \quad (10)$$

denote two distinct *column sums* of volume fractions from the 3×3 block of cells $B_{ij} = [x_{i-1}, x_{i+2}] \times [y_{j-1}, y_{j+2}]$ centered on the ij -th cell C_{ij} .

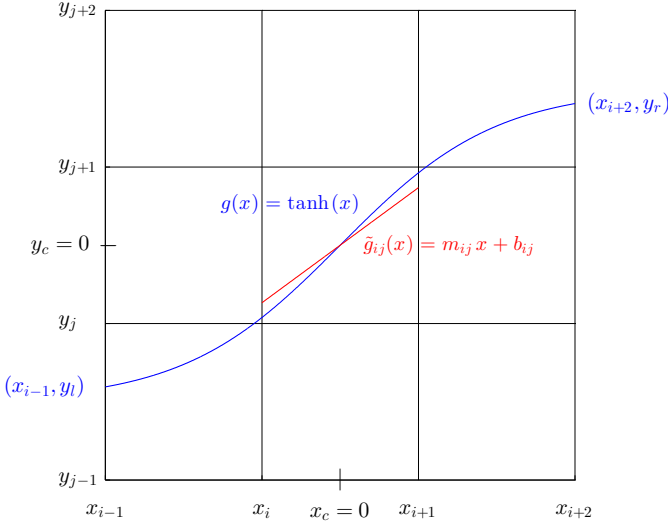


Figure 1. In this example the interface is $g(x) = \tanh(x)$ and all three of the column sums S_{i-1} , S_i , and S_{i+1} are *exact*. The linear approximation $\tilde{g}_{ij}(x) = m_{ij}x + b_{ij}$ in the center cell C_{ij} is also plotted, where the slope m_{ij} is given by (9) with $\alpha = 1$ and $\beta = -1$ and b_{ij} is determined by the constraint $\Lambda_{ij}(\tilde{g}) = \Lambda_{ij}(g)$ in (8).

For $\alpha = -1, 0, 1$ the column sum $S_{i+\alpha}$ is said to be *exact* if

$$S_{i+\alpha} = \frac{1}{h^2} \int_{x_{i+\alpha}}^{x_{i+\alpha+1}} (g(x) - y_{j-1}) dx. \quad (11)$$

and *exact to $O(h)$* if

$$\left| S_{i+\alpha} - \frac{1}{h^2} \int_{x_{i+\alpha}}^{x_{i+\alpha+1}} (g(x) - y_{j-1}) dx \right| \leq \bar{C} \kappa_{\max} h, \quad (12)$$

where $\bar{C} > 0$ is a constant, defined in (53) below, which is independent of h and κ_{\max} . Column sums are discussed in greater detail in Section 2.2.

(V) Each of the two column sums $S_{i+\alpha}$ and $S_{i+\beta}$ in (9), where $\alpha \neq \beta$, is either exact or exact to $O(h)$. Thus, by Theorem 23 of [23] the slope m_{ij} defined in (9) is a first-order accurate approximation to $g'(x_c)$,

$$|m_{ij} - g'(x_c)| \leq \bar{C} \kappa_{\max} h, \quad (13)$$

where x_c denotes the center of the interval $[x_i, x_{i+1}]$. It then follows from Theorem 4 on page 152 below that the approximation \tilde{g} defined in (7)–(10) is a second-order accurate approximation to g in C_{ij} ; i.e., the bound in (4) holds in C_{ij} .

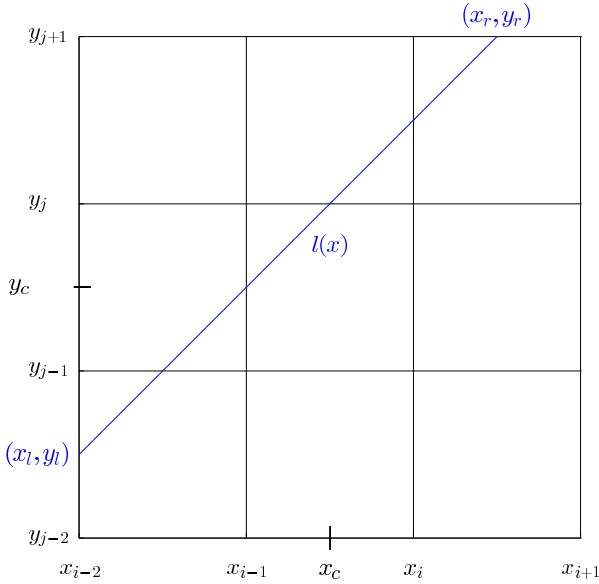


Figure 2. In this example the interface is a line $l(x) = mx + b$ that has two exact column sums, S_{i-1} and S_i , in the first and second columns of the 3×3 block of cells B_{ij} centered on the cell C_{ij} . In this case the slope m_{ij} defined in (9) with $\alpha = 0$ and $\beta = -1$ is *exactly* equal to the slope m of the interface: $m_{ij} = m$. It is always the case if the true interface is a line; then one of the four standard rotations of B_{ij} about its center will orient the block so at least one of the divided differences of the column sums in (9) is exact and hence, the approximation \tilde{g}_{ij} to the interface in the center cell C_{ij} defined in (7)–(10) will exactly equal the interface in that cell, $\tilde{g}_{ij}(x) = m_{ij}x + b_{ij} = mx + b = l(x)$. In other words, the approximation \tilde{g}_{ij} defined in (7)–(10) will *always* reconstruct a linear interface exactly.

1.1. Remarks concerning conditions (I)–(V).

(1) The proof of (4) is based on showing if the constraint in (5)–(6) holds, then for all cells C_{ij} that contain a portion of the interface, there are at least two distinct column sums $S_{i+\alpha}$ and $S_{i+\beta}$, with $\alpha \neq \beta$, which are either exact or exact to $O(h)$ in one or more of the four standard rotations of the 3×3 block of cells B_{ij} centered on C_{ij} . An algorithm for determining which of the four standard rotations of the block B_{ij} has this property is described in Section 2.1.

(2) The constraint on h in (5) may be viewed as dictating the number of cells required to produce a pointwise second-order accurate approximation to a circle of radius r on a grid with cell size h . To see this, note the curvature of the circle is $\kappa_{\max} = r^{-1}$ and hence, by (5) and (6), one must have

$$16.5h = C_h^{-1}h \leq r. \tag{14}$$

This implies one needs a 35×35 square block of cells covering the circle (this includes a border one cell wide outside the circle) in order to ensure the piecewise

linear approximation defined in (7)–(10) is a pointwise second-order accurate approximation to the circle in each cell C_{ij} that contains a portion of the circle.

This could be an overestimate of the number of cells required to achieve pointwise second-order accuracy. However, if this is so, then it is likely one will need to employ ideas other than the ones presented in this article, and in [23], in order to obtain a better result; that is, a larger value for C_h , thereby implying fewer cells are required to reconstruct a circle of radius r to pointwise second-order accuracy in h . In other words, the constant of proportionality C_h in (6) appears to be optimal in the sense that it is about as large as one can obtain with the ideas and techniques presented here and in [23].

(3) In [23] the constraint that corresponds to (5) is

$$h \leq \min\{\tilde{C}_h \kappa_{\max}^{-1}, \kappa_{\max}^{-2}\}, \quad (15)$$

where

$$\tilde{C}_h \stackrel{\text{def}}{=} \bar{C}_h[4] = \frac{\sqrt{4} - \sqrt{2}}{4\sqrt{2}\sqrt{4-1}} = \frac{\sqrt{2} - 1}{4\sqrt{3}}, \quad (16)$$

where $\bar{C}_h[a]$ is defined in Equation (A.1) in the Appendix. The principal new result of this article is the elimination of the much more restrictive (and dimensionally inconsistent) constraint

$$h \leq \kappa_{\max}^{-2} \quad (17)$$

in (15). Thus, for a given interface z , one can reconstruct z to second-order in h using a larger value of h than dictated by (17). A notable consequence of this new proof is that the bound on the error in (4) depends linearly on κ_{\max} .

A minor change from [23] is the very slight increase in the value of C_h from $C_h = \tilde{C}_h \approx (16.73)^{-1}$ to $C_h = 2/33 = (16.5)^{-1}$. The reason for this change is solely for the purpose of presenting the example in item (2) above in terms of an integral number of grid cells. The details concerning how C_h and \tilde{C}_h are chosen appear in the Appendix.

The majority of the work in this article is concerned with proving the more restrictive constraint in (17) is unnecessary. This involves replacing the arguments in Sections 3.2–3.4 of [23] with those in Section 4 here. Sections 2.2.2 and 3 of this article contain a more detailed discussion of the modifications to the argument in [23] required to eliminate the constraint in (17).

Although it is not necessary to modify the argument in [23] in order to *increase* the value of C_h from $(\sqrt{2} - 1)/(4\sqrt{3}) \approx (16.73)^{-1}$ to $C_h = 2/33 = (16.5)^{-1}$, a more general version of Theorem 6 from [23] is presented as Theorem A.1 in the Appendix in order to clearly show the considerations that influence the choice of C_h .

(4) **Figure 1** contains an example of the volume-of-fluid approximation $\tilde{g}_{ij}(x) = m_{ij}x + b_{ij}$ defined in (7)–(10) to the interface $g(x) = \tanh(x)$ in the center cell C_{ij} of a 3×3 block of cells in which all three column sums are exact. Hence, \tilde{g}_{ij} is a pointwise second-order accurate approximation to g for any choice of $\alpha, \beta = 1, 0, -1$ with $\alpha \neq \beta$ in (9) provided b_{ij} is chosen so (8) holds, where $\Lambda_{ij}(g)$ is the volume fraction in C_{ij} lying under the curve g .

Figure 2 contains an example of a linear interface $l(x) = mx + b$ in which only two of the column sums, namely, S_{i-1} and S_i , are exact, yet the approximate interface $\tilde{g}_{ij} = m_{ij}x + b_{ij}$, *exactly reproduces the line l* if m_{ij} is given by (9) with $\alpha = 0$ and $\beta = -1$ and b_{ij} is chosen so $\Lambda_{ij}(\tilde{g}) = \Lambda_{ij}(l)$ where $\Lambda_{ij}(l)$ is the volume fraction in C_{ij} lying below the line l . (See **Example 1** on page 136 for additional details.)

Figure 3 contains an example of the arc of a circle, $c_\epsilon(x)$ that passes through the center cell C_{ij} of the 3×3 block B_{ij} , but for which the center column sum

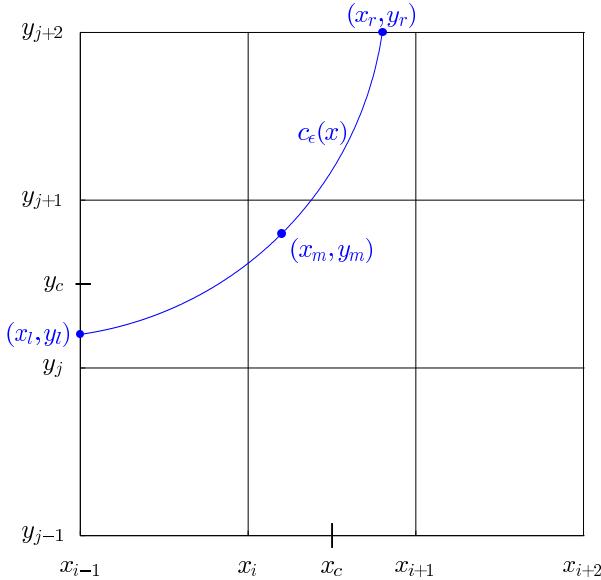


Figure 3. This figure contains an example of an interface $c_\epsilon(x)$, which is a circle that satisfies (5)–(6), but for which the center column sum is not exact in any of the four standard rotations of the 3×3 block of cells B_{ij} centered on the cell C_{ij} . Consequently, the only reasonable approximation m_{ij} to $c'_\epsilon(x_c)$ of the form (9) is with $\alpha = 0$ and $\beta = -1$, which must necessarily have a nonexact center column sum S_i . By **Theorem 3** below, which is the basis for the principal result of this article, if the constraint in (5) and (6) is satisfied, then the center column sum S_i *must be exact to $O(h)$* . In other words, in this case the constraint in (5)–(6) implies (12) (with $\alpha = 0$) must hold. This is sufficient to prove (13), namely, $|m_{ij} - c'_\epsilon(x_c)| \leq \bar{C}\kappa_{\max}h$, which is Theorem 23 of [23]. Finally, by **Theorem 4**, the approximate interface $\tilde{g}_{ij}(x)$ with the slope m_{ij} as given above must be a second-order accurate approximation to $c_\epsilon(x)$ in the max norm.

S_i is not exact. However, by [Theorem 3](#) below, S_i is exact to $O(h)$, as defined in [\(12\)](#). It follows from [Theorem 23](#) of [\[23\]](#) and [Theorem 4](#) in this article that the approximation to the interface $\tilde{g}_{ij}(x)$, with the slope m_{ij} given by [\(9\)](#) with $\alpha = 0$ and $\beta = -1$, will still be pointwise second-order accurate in h , even though S_i is only exact to $O(h)$.

The convention followed in each of these examples is that material 1 *lies below* the interface. However, in practice the 3×3 block B_{ij} centered on a cell C_{ij} containing a portion of the interface can have material 1 lying above, below, to the right or to the left of the interface. In [Section 2.1](#) I present an algorithm for determining which of the four standard rotations of the 3×3 block of cells B_{ij} , namely, rotation clockwise by 0, 90, 180, or 270 degrees, will orient the block B_{ij} so material 1 lies below the interface.

[Theorem 4](#), which is the main result of this article, follows from proving that if [\(5\)–\(6\)](#) holds, then in at least one of these four standard orientations of the block B_{ij} there will always exist at least one column sum that is exact and a second column sum that is either exact or exact to $O(h)$. A more detailed discussion of these issues is contained in [Section 3](#).

[Figure 1](#) contains an example in which one orientation of B_{ij} contains three exact column sums. [Figure 2](#) contains an example in which in two different orientations of B_{ij} contain two exact column sums. [Figure 3](#) contains an example in which in two different orientations B_{ij} contain one exact column sum and one column sum that is exact to $O(h)$. (Note: rotation of the block B_{ij} in [Figure 3](#) by 180 or 270 degrees clockwise results in a configuration in which material 1 lies *above* the interface and therefore, neither [\(11\)](#) nor [\(12\)](#) is true.)

(5) The constraint in [\(5\)–\(6\)](#) is sufficient to ensure *filaments* or *fingers* of the type shown in [Figure 4](#) will not occur on a grid with cell size h where κ_{\max} is the maximum magnitude of curvature of the filament. In this article I have not attempted to catalog all of the ways in which a filament of width $w < h$ can occur in an arbitrary C^2 simple closed curve lying in the domain Ω . It could be that the constraint in [\(5\)–\(6\)](#) is sufficient to ensure if the interface is a simple closed curve in Ω , then all such filaments will be resolved to pointwise second-order accuracy in h . However, I have not attempted to prove this here. The result in this article concerning filaments of the type illustrated in [Figure 4](#) is only a *local* result. In other words, in all of what follows I am explicitly excluding interfaces \mathbf{z} such that for two disjoint intervals (s_l, s_r) and $(\tilde{s}_l, \tilde{s}_r)$ the two *separate* portions of the interface $\mathbf{z}(s) = (x(s), y(s))$ for $s_l < s < s_r$ and $\mathbf{z}(\tilde{s}) = (x(\tilde{s}), y(\tilde{s}))$ for $\tilde{s}_l < \tilde{s} < \tilde{s}_r$, occupy the same 3×3 block of cells B_{ij} .

1.2. The volume-of-fluid interface reconstruction problem. Consider the following problem. Given only the collection of volume fractions Λ_{ij} in the grid Ω^h

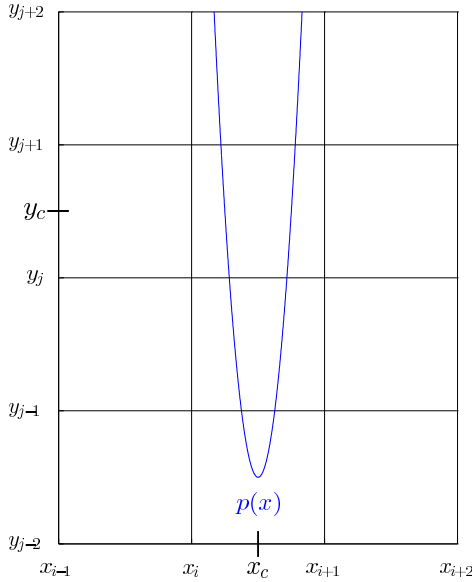


Figure 4. The interface $p(x)$ is a model of a *filament* of material 2 contained entirely within the center column of the 3×4 block of cells $[x_{i-1}, x_{i+2}] \times [y_{j-2}, y_{j+1}]$. In this example $h = 1$, the interface is the parabola $p(x) = 32(x - x_c)^2 + (y_{j-1} - h/2)$ and hence, it follows that κ_{\max} does not satisfy the constraint in (5)–(6), since $\kappa_{\max} = 64 > 2/(33h) = C_h/h$. This indicates the filament is underresolved on this grid. In general, the constraint in (5)–(6) ensures the interface does not have sharp or “hairpin” turns on the scale h of the cell in which one wants to reconstruct the interface.

covering Ω , *reconstruct* $\mathbf{z}(s)$ in the following way. For each cell C_{ij} in Ω^h for which $0 < \Lambda_{ij} < 1$, find a piecewise linear approximation $\tilde{\mathbf{z}}$ to \mathbf{z} as shown, for example, in Figure 1. Furthermore, the approximate interface $\tilde{\mathbf{z}}$ must have the property that the volume fractions $\tilde{\Lambda}_{ij}$ due to $\tilde{\mathbf{z}}$ are identical to the volume fractions Λ_{ij} due to \mathbf{z} ,

$$\tilde{\Lambda}_{ij} = \Lambda_{ij} \quad \text{for all cells } C_{ij} \text{ in } \Omega^h. \tag{18}$$

An algorithm for finding such an approximation is known as a *piecewise linear* volume-of-fluid interface reconstruction method. More generally, there are volume-of-fluid interface reconstruction methods that produce other types of approximations to the interface, such as with piecewise constant [18; 19] and piecewise parabolic [26] functions. However, this article is only concerned with piecewise linear approximations to the interface of the form (7).

Although these algorithms have historically been known as “volume-of-fluid” methods, one can use them to model the interface between any two (or more) materials, including two gases [7], a gas (or vacuum) and a solid [25], a liquid and a solid [14], two solids and vacuum [15; 16], or any other combination of materials.

The design of volume-of-fluid interface reconstruction methods for reconstructing multiple interfaces in problems with more than two materials, especially a large number of distinct materials, is currently a very active area of research.

The property (18) that $\tilde{\Lambda}_{ij} = \Lambda_{ij}$ in all cells in Ω^h is the principal feature that distinguishes volume-of-fluid interface reconstruction methods from other interface reconstruction or tracking methods. It ensures the computational value of the total volume of each material is *exact* to within machine precision. In other words, all volume-of-fluid interface reconstruction methods are conservative in that they conserve the volume of each material in the computation. This is essential if the interface reconstruction method is part of a conservative finite difference method designed to approximate solutions of a system of hyperbolic conservation laws since, for example, in order to obtain the correct shock speed it is necessary for all of the conserved quantities to be conserved by the underlying numerical method (e.g., see [12]). More generally, a necessary condition for the numerical method to converge to the correct weak solution of a system of hyperbolic conservation laws is all of the quantities conserved in the system of conservation laws must also be conserved by the numerical method [11; 13].

Volume-of-fluid methods have been used by researchers to track material interfaces since at least the mid 1970s (e.g., [18; 19]). Researchers have developed a variety of volume-of-fluid algorithms for modeling everything from flame propagation [4] to curvature and solidification [5]. In particular, the problem of developing high-order accurate volume-of-fluid methods for modeling the curvature and surface tension of an interface has received a lot of attention [1; 3; 5; 6; 9; 32; 22; 26]. Volume-of-fluid methods were among the first algorithms to be implemented in codes developed at national laboratories, both in the US [8; 10; 17; 18; 30; 31] and elsewhere [20; 33; 34; 35], for tracking interfaces in a variety of difficult fluid flow and material deformation problems.

The present article is only concerned with the accuracy one can obtain using a volume-of-fluid interface reconstruction algorithm to approximate a given *stationary* interface $z(s)$. The related problem of approximating the movement of the interface in time, for which one would use a *volume-of-fluid advection algorithm* is not addressed here. See, for example, [2; 21; 26; 27; 28] for a description and analysis of several such algorithms.

2. Essential background material

2.1. Rotation and/or reflection of the 5×5 block of cells \tilde{B}_{ij} . Given a cell C_{ij} that contains a portion of the interface it is expedient to consider the 5×5 block of cells \tilde{B}_{ij} centered on C_{ij} rotated clockwise by 0, 90, 180, or 270 degrees about (x_c, y_c) and/or reflected about the vertical line $x = x_c$ or the horizontal line $y = y_c$.

where (x_c, y_c) is the center of the cell C_{ij} as shown in Figures 2, 3 and 4. (Figure 1 on page 203 of [24] contains an illustration of the 5×5 block of cells \tilde{B}_{ij} .) This is because, with the proper choice of one of these four rotations, one can orient the block \tilde{B}_{ij} so the interface can either be written as a single-valued function $y = g(x)$ or $x = G(y)$ of the independent variable x (resp. y) such that in this new coordinate frame the column sum S_i corresponds to the integral of $g(x) - y_{j-1}$ (resp. $G(y) - x_{i-1}$) over the interval $[x_i, x_{i+1}]$ (resp. $[y_j, y_{j+1}]$) and similarly for the column sums S_{i-1} and S_{i+1} . I use the reflection about the line $x = x_c$ to transform cases such as the reflection of the case shown in Figure 3 about the line $x = x_c$ into the case shown in Figure 3, and similarly for reflections about the line $y = y_c$. This enables one to reduce all of the various ways the interface can enter the 3×3 block of cells B_{ij} , pass through the center cell C_{ij} , and leave the block B_{ij} to two canonical cases, namely, Configuration A and Configuration B below.

It is important to note one does not need to perform these coordinate transformations in order to *prove* the piecewise linear volume-of-fluid interface reconstruction algorithm defined in (7)–(10) produces a second-order accurate approximation to the exact interface. Rather, these coordinate transformations are simply an expedient that allows one to reduce consideration of all of the various ways the interface can enter B_{ij} , pass through C_{ij} , and then leave B_{ij} to two canonical cases. This is a consequence of the symmetry lemma on page 119 of [24], from which it follows that all such configurations of the interface with respect to the 3×3 block of cells B_{ij} are equivalent to one of the following two cases.¹

Configuration A: The interface enters B_{ij} across its left edge and exits across its right edge as shown, for example, in Figure 1. In this case the best slope for one to use is m_{ij} defined by $\alpha = 1$ and $\beta = -1$ in (9), although either of the other two slopes given by $\alpha = 0$ and $\beta = -1$ or $\alpha = 1$ and $\beta = 0$ will also furnish a pointwise second-order accurate approximation of the form (7)–(10) to the interface in the center cell C_{ij} .

Configuration B: The interface enters B_{ij} across its left edge and exits across its top edge as shown, for example, in Figures 2 and 3. In this case one *must* use the slope m_{ij} in (9) with $\alpha = 0$ and $\beta = -1$ in order to produce a pointwise second-order accurate approximation of the form (7)–(10) to the interface in the center cell C_{ij} .

¹The symmetry lemma in [23] ensures that if (5)–(6) holds, then each of the ways the interface can enter the block B_{ij} , pass through the center cell C_{ij} , and exit B_{ij} is equivalent to one of four canonical cases: I–IV. By Lemma 11 in [23] Case I cannot occur and a rotation of the block B_{ij} clockwise by 90° transforms Case III into Case II, thereby leaving only Case II, which is Configuration A, and Case IV, which is Configuration B.

Note that each 5×5 block of cells \tilde{B}_{ij} centered on a cell C_{ij} containing a portion of the interface will have its own rotation and/or reflection; that is, the rotation and/or reflection is only performed *locally*, solely for the purpose of determining the slope m_{ij} of the approximate interface in the ij -th cell C_{ij} . Different rotations and/or reflections will, in general, be required for different 5×5 blocks of cells centered on different cells C_{ij} that contain parts of the interface. Furthermore, one only uses these coordinate transformations to determine a first-order accurate approximation m_{ij} to $g'(x_c)$ in the center cell. The grid Ω^h covering the domain Ω always remains the same. Thus, if one is using the interface reconstruction algorithm as part of a numerical method to solve a more complex problem than the one posed here, e.g., the movement of a fluid interface where the underlying fluid flow is a solution of the Euler or Navier–Stokes equations, it is not necessary to perform a coordinate transformation on the underlying numerical fluid flow solver.

There are a variety of techniques for determining which of the four rotations and which reflection, if any, will orient the 3×3 block B_{ij} so the interface can be written as a single-valued function of one of the independent variables x or y , such that in the rotated coordinates the column sum S_i corresponds to the integral of $g(x) - y_{j-1}$ (resp. $G(y) - x_{i-1}$) over the interval $[x_i, x_{i+1}]$ (resp. $[y_j, y_{j+1}]$) and similarly for the column sums S_{i-1} and S_{i+1} . The simplest technique is probably the algorithm described in Section 3 of [24], a variation of which I will now describe.

Step I: Given a cell C_{ij} that contains a portion of the interface $\mathbf{z}(s)$, or equivalently, a cell C_{ij} in which $0 < \Lambda_{ij} < 1$, rotate the 5×5 block of cells \tilde{B}_{ij} centered on C_{ij} together with their associated volume fractions by 0, 90, 180, or 270 degrees so in the *rotated coordinate frame* the bottom row of cells in the 5×5 block \tilde{B}_{ij} satisfy

$$\Lambda_{i-2,j-2} = 1, \quad \Lambda_{i-1,j-2} = 1, \quad \Lambda_{i,j-2} = 1, \quad \Lambda_{i+1,j-2} = 1, \quad \Lambda_{i+2,j-2} = 1.$$

This ensures that the interface does not cross the bottom edge of the 3×3 block of cells B_{ij} .

Step II: Now examine the left and right edges of the 5×5 block of cells \tilde{B}_{ij} . If

$$\Lambda_{i-2,j-2} = 1, \quad \Lambda_{i-2,j-1} = 1, \quad \Lambda_{i-2,j} = 1, \quad \Lambda_{i-2,j+1} = 1, \quad \Lambda_{i-2,j+2} = 1,$$

then the interface must cross the top and right-hand edges of the 3×3 block of cells B_{ij} . In this case reflect the cells together with their associated volume fractions about the vertical line $x = x_c$ in order to orient the block \tilde{B}_{ij} so the interface only crosses the left-hand and top edges of the 3×3 block B_{ij} as shown in Figures 2 and 3. (Lemma 11 of [23] ensures any interface of the form $y = g(x)$ on the interval $[x_{i-1}, x_{i+2}]$ or $x = G(y)$ on the interval $[y_{j-1}, y_{j+2}]$ that satisfies the constraint

in (5)–(6) cannot enter the block B_{ij} across a given edge, pass through the center cell C_{ij} , and then exit B_{ij} across the same edge.)

Not only does this procedure reduce the number of cases one must consider during the course of proving the results in this article and those in [23], it also reduces the number of cases one must consider in the implementation of the algorithm described in [24]. In all of what follows I will express the interface as $y = g(x)$ and, unless noted otherwise, the coordinates of the edges of the cells in the 3×3 block B_{ij} centered on a cell C_{ij} containing the interface will be denoted by x_{i-1} , x_i , x_{i+1} , x_{i+2} and y_{j-1} , y_j , y_{j+1} , y_{j+2} , with it being understood that a transformation of the coordinate system as described above may have been performed in order for this representation of the interface to be valid, and that the names of the variables x and y might have been interchanged in order to write the interface as $y = g(x)$.

2.2. Column sums. Let C_{ij} be a cell such that $0 < \Lambda_{ij} < 1$ and assume the 3×3 block of cells B_{ij} centered on C_{ij} has been rotated by 0, 90, 180, or 270 degrees as described above, so the interface $z(s)$ can be expressed as a single-valued function $y = g(x)$ or $x = G(y)$ of the independent variable x (resp. y). Thus, in this new coordinate frame the column sum S_i corresponds to the integral of $g(x) - y_{j-1}$ (resp. $G(y) - x_{i-1}$) over the interval $[x_i, x_{i+1}]$ (resp. $[y_j, y_{j+1}]$) and similarly for the column sums S_{i-1} and S_{i+1} . The accuracy of the piecewise linear approximation to the interface in C_{ij} defined in (7)–(10) depends entirely on the accuracy with which the column sums S_{i-1} , S_i and S_{i+1} approximate the volume / area under the interface in their respective columns from the base $y = y_{j-1}$ of the block B_{ij} to the interface. The purpose of this section is to give the reader an understanding of why this must be so.

2.2.1. Exact column sums. Consider the three columns in the 3×3 block of cells B_{ij} centered on the cell C_{ij} . The column sums S_{i-1} , S_i , and S_{i+1} are a nondimensional way of storing the total volume / area of material 1 in these three columns. In order to approximate the portion of the interface $g(x)$ in the ij -th cell C_{ij} to second-order in h with the piecewise linear function $\tilde{g}_{ij}(x)$ defined in (7), one must use two of the three column sums in B_{ij} to compute the slope m_{ij} of $\tilde{g}_{ij}(x)$ as illustrated in the examples in Figures 1 and 2.

To see why this is so, consider an arbitrary column consisting of three cells with left edge $x = x_i$ and right edge $x = x_{i+1}$ and assume the interface can be written as a function $y = g(x)$ on the interval $[x_i, x_{i+1}]$. Assume also the interface enters the column through its left edge and exits the column through its right edge and does not cross the top or bottom edges of the column as, for example, is the case for each of the three columns in the 3×3 block of cells in Figure 1. Then the total volume / area of material 1 that occupies the three cells in this particular column and lies below the interface $g(x)$ is equal to the integral of $g(x) - y_{j-1}$ over the

interval $[x_i, x_{i+1}]$. Thus, (11) holds; in other words, the i -th column sum S_i is exact.

Exact column sums are the key to ensuring a volume-of-fluid interface reconstruction algorithm of the form defined in (7)–(10) is second-order accurate. Given the 3×3 block of cells B_{ij} centered on a cell C_{ij} that contains a portion of the interface $y = g(x)$, the main result in this article, [Theorem 4](#), is based on how well the column sums S_{i-1} , S_i and S_{i+1} approximate the *normalized* integral of g in that particular column,

This is because, by (9), the slope m_{ij} of the piecewise linear approximation \tilde{g}_{ij} to the interface g in C_{ij} will be the divided difference of two of these column sums. In other words, m_{ij} is chosen to be one of the following three quantities:

$$m_{ij}^l = (S_i - S_{i-1}), \quad (19a)$$

$$m_{ij}^c = \frac{(S_{i+1} - S_{i-1})}{2}, \quad (19b)$$

$$m_{ij}^r = (S_{i+1} - S_i). \quad (19c)$$

A consequence of [Theorem 23](#) in [23] is if two of the column sums $S_{i+\alpha}$ and $S_{i+\beta}$ for some $\alpha, \beta = 1, 0, -1$ with $\alpha \neq \beta$ are exact, then the slope m_{ij} in (9) must satisfy (13). Consequently, by [Theorem 4](#) below, which is a stronger version of [Theorem 24](#) in [23], the piecewise linear approximation $\tilde{g}_{ij}(x)$ defined in (7)–(10) will be a pointwise second-order accurate approximation to the true interface $g(x)$ for all $x \in [x_i, x_{i+1}]$. In fact, $\tilde{g}_{ij}(x)$ will be a pointwise second-order accurate approximation to $g(x)$ for all $x \in [x_{i-1}, x_{i+2}]$, albeit with a slightly larger constant multiplying $\kappa_{\max} h^2$.

Example 1. In order to see why the divided difference of two exact column sums must produce a slope m_{ij} that is a first-order accurate approximation to $g'(x_c)$, the slope of the interface at the center of the interval $[x_i, x_{i+1}]$, consider the case of a linear interface $l(x) = mx + b$ as shown in [Figure 2](#). In this particular orientation of the 3×3 block of cells B_{ij} the interface g has two exact column sums; namely, the first and second ones, S_{i-1} and S_i , where S_i denotes the column sum associated with the interval $[x_i, x_{i+1}]$ and S_{i-1} denotes the column sum associated with the interval $[x_{i-1}, x_i]$. It is easy to check that

$$\begin{aligned} m &= \frac{1}{h^2} \int_{x_i}^{x_{i+1}} (l(x) - y_{j-1}) dx - \frac{1}{h^2} \int_{x_{i-1}}^{x_i} (l(x) - y_{j-1}) dx \\ &= (S_i - S_{i-1}) = m_{ij}^l. \end{aligned}$$

In this example the divided difference m_{ij}^l in (19a) of the column sums S_{i-1} and S_i is *exactly* equal to the slope m of the linear interface $l(x) = mx + b$ and hence,

since (8) must also hold, the piecewise linear approximation $\tilde{g}_{ij}(x)$ defined in (7) coincides with the true interface $l(x)$ in C_{ij} ,

$$|l(x) - \tilde{g}_{ij}(x)| = 0 \quad \text{for all } x \in [x_i, x_{i+1}].$$

If the exact interface is a line, then it is always the case that in one of the four standard rotations of the 3×3 block of cells B_{ij} at least one of the divided differences of the column sums in (19) is exact. For example, note that in the case shown in Figure 2 one can rotate the 3×3 block of cells B_{ij} 90 degrees clockwise and in this new orientation the correct slope to use when forming the piecewise linear approximation $\tilde{g}_{ij}(x) = m_{ij} + b_{ij}$ to the line $l(x) = mx + b$ will be $m_{ij} = m_{ij}^r$ as defined in (19c), which again exactly equals the slope m of $l(x)$.

Of course, in general, the divided difference of two of the column sums will not be precisely equal to the slope of the interface at the midpoint x_c of the interval $[x_i, x_{i+1}]$ as in the preceding example. However, as a consequence of Theorem 3 below, and Theorem 23 of [23], if h satisfies (5)–(6), one can always find an orientation of the 3×3 block of cells B_{ij} such that at least two of the column sums are sufficiently accurate that one of the divided differences in (19) satisfies (13).

Once one has chosen an orientation of the 3×3 block of cells B_{ij} such that at least two of the column sums are sufficiently accurate that one of the divided differences in (19) satisfies (13), one uses the constraint in (8), namely, $\Lambda_{ij}(\tilde{g}) = \Lambda_{ij}(g)$, to form the piecewise linear approximation $\tilde{g}_{ij}(x) = m_{ij}x + b_{ij}$ to the interface. In other words, given m_{ij} , the constraint $\Lambda_{ij}(\tilde{g}) = \Lambda_{ij}(g)$ determines b_{ij} .

2.2.2. Column sums that are exact to $O(h)$. One might expect there exists a value of C_h that will ensure if the cell size h satisfies the constraint in (5)–(6), then after one of the four standard rotations of the 3×3 block B_{ij} about its center, the block will always have at least two exact column sums. Unfortunately, as the following example demonstrates, there is no bound of the form (5)–(6) which, for a fixed h , will ensure a C^2 interface will always have at least two exact column sums in one of the four standard orientations of the grid.

Example 2. Consider the curve $c_\epsilon(x)$ shown in Figure 3 where $0 < \epsilon < h$ is a small parameter. One can always find a circle $c_\epsilon(x)$ that passes through the three noncollinear points $(x_l, y_l) = (x_{i-1}, y_j + \epsilon)$, $(x_m, y_m) = (x_i + \epsilon, y_{j+1} - \epsilon)$ and $(x_r, y_r) = (x_{i+1} - \epsilon, y_{j+2})$ as shown in the figure. As $\epsilon \rightarrow 0$ the arc of the circle passing through (x_l, y_l) , (x_m, y_m) and (x_r, y_r) tends to the chord connecting (x_l, y_l) and (x_r, y_r) which, since the curvature of the chord is 0, implies the radius r^ϵ of $c_\epsilon(x)$ tends to ∞ . Therefore, no matter how small one chooses C_h there exists $\epsilon_0 > 0$, such that the radius r^ϵ satisfies $h \leq C_h r^\epsilon$, or equivalently, $h \leq C_h (\kappa_{\max}^\epsilon)^{-1}$ for all $\epsilon \leq \epsilon_0$. Hence, for $\epsilon \leq \epsilon_0$ the circle $c_\epsilon(x)$ satisfies (5)–(6). However, since by construction $y_j < y_l$ and $x_r < x_{i+1}$, the center column sum will not be exact

in any of the four standard orientations of the block B_{ij} . Consequently, if one wants to construct an approximation to $c_\epsilon(x)$ based solely on the volume fraction information contained in the 3×3 block B_{ij} centered on the cell C_{ij} that contains the point (x_m, y_m) on the interface $c_\epsilon(x)$, the best result one can hope for is that the center column sum S_i is exact to $O(h)$ in the sense defined in (12).

All of the work in Sections 4.1 to 4.3 of this article is devoted to proving if (5)–(6) holds, then in cases such as the one shown in Figure 3 the error between the column sum S_i and the normalized integral of the interface $g(x)$ in that column is $O(h)$; i.e., the inequality in (12) holds with $\alpha = 0$, where $\bar{C} > 0$, defined in (53) below, is a global constant independent of h and κ_{\max} .

In [23], in order to prove if the center cell S_i is not exact, but is exact to $O(h)$, then one of the divided differences m_{ij}^l or m_{ij}^r is still sufficiently accurate that (13) must hold, it was necessary to have a more stringent restriction on the cell size than one of the form (5)–(6).² This restriction was $h \leq \kappa_{\max}^{-2}$, which for κ_{\max} large enough is more restrictive than the constraint in (5)–(6). In all of the other ways in which the interface enters the 3×3 block B_{ij} , passes through the center cell C_{ij} and exits the block B_{ij} , the constraint in (5)–(6) is sufficient to prove there is an orientation of B_{ij} such that at least two of the column sums are *exact*, and hence one of the divided differences in (19) satisfies (13). The primary purpose of this article is to prove if the center column sum S_i is not exact the more restrictive constraint $h \leq \kappa_{\max}^{-2}$ is not necessary. In other words, if the exact interface g satisfies (5)–(6), then for every cell C_{ij} that contains a portion of the interface, after one of the four standard rotations of the 3×3 block B_{ij} about its center (x_c, y_c) there are at least two column sums that are sufficiently accurate (meaning either exact or exact to $O(h)$), that one of the divided differences in (19) satisfies (13).

The purpose of this article is to show the constraint in (5)–(6) is sufficient to ensure in cases such as the one shown in Figure 3, the error between the center column sum S_i and the normalized integral of the interface g in the center column satisfies (12) with $\alpha = 0$ and hence, the error in the approximation m_{ij}^l to the slope $g'(x_c)$ is small enough that (13) still holds. Once this is done, by (13) the slope m_{ij}^l is a first-order accurate approximation to the first derivative $g'(x_c)$ of the interface at the center x_c of the interval $[x_i, x_{i+1}]$. One can then show the piecewise linear

²A consequence of the proof of Theorem 10 in [23] is if the interface satisfies (5)–(6) and passes through the center cell C_{ij} of the 3×3 block of cells B_{ij} , then after one of the four standard rotations of B_{ij} about its center, either the left or right column sum must be exact. If it is the right column sum S_{i+1} that is exact, then reflection of the block B_{ij} about the vertical line $x = x_c$ results in the block being oriented so the left column sum S_{i-1} is now exact as shown in Figure 3. Thus, it is only necessary to consider the case in which the center column sum S_i is exact to $O(h)$ and the left column sum S_i is exact, as illustrated in Figure 3.

approximation $\tilde{g}_{ij}(x) = m_{ij}^l x + b_{ij}$ is a second-order accurate approximation to the interface $g(x)$ on the interval $[x_i, x_{i+1}]$. This is [Theorem 4](#).

3. An overview of the structure of the proof

Sections 3 and 4 of [\[23\]](#) contain a proof of the following. If h satisfies the constraint in [\(15\)](#), then by rotating the 3×3 block of cells B_{ij} centered on C_{ij} by 0, 90, 180, or 270 degrees clockwise, one can find a coordinate frame in which there are at least two distinct column sums $S_{i+\alpha}$ and $S_{i+\beta}$ such that their divided difference [\(9\)](#) satisfies [\(13\)](#). Section 3.1 of [\[23\]](#) contains a proof that the constraint $h \leq \tilde{C}_h \kappa_{\max}^{-1}$, where \tilde{C}_h is defined in [\(A.6\)](#), is sufficient to ensure the interface has two *exact* column sums *in all but one of the ways* in which the interface g enters the 3×3 block of cells B_{ij} , passes through its center cell C_{ij} , and exits B_{ij} . The exception is the case in which the center column sum S_i is not exact, but only exact to $O(h)$, as illustrated in [Figure 3](#). Sections 3.2–3.4 of [\[23\]](#) are devoted to proving that, in this latter case, the center column sum S_i is exact to $O(h)$. However, the proof requires the second of the two constraints in [\(15\)](#) above, namely $h \leq \kappa_{\max}^{-2}$, to hold.

The purpose of [Section 4](#) is to prove the weaker constraint in [\(5\)](#), with C_h defined in [\(6\)](#), is sufficient to ensure that in cases such as the one described above, the center column sum S_i is exact to $O(h)$. This, together with the results from [Section 4](#) of [\[23\]](#), ensure the approximation $\tilde{g}_{ij}(x)$ in [\(7\)](#) is a second-order accurate approximation in the max norm to $g(x)$ on the interval $[x_i, x_{i+1}]$.

[Theorem 4](#) in [Section 5](#), which is the main result of this article, is a stronger version of [Theorem 24](#) of [\[23\]](#). Namely, if $h \leq C_h \kappa_{\max}^{-1}$, then [\(4\)](#) holds. This theorem is based on the results in [Section 4](#) below.

The terms in the error bound on the right-hand side of [\(4\)](#) that have changed from [Theorem 24](#) of [\[23\]](#) are the positive constants κ_{\max} and C_m . In particular, the linear dependence on κ_{\max} of the max norm of the difference $z - \tilde{z}$ is explicitly displayed in the present article. In [\[23\]](#) the constant C_m was of the form $50\kappa_{\max}/3 + C_S$, where C_S is a constant, which is independent of κ_{\max} and h . The new value of C_m is defined in [\(59\)](#) below.

4. The center column sum S_i is exact to $O(h)$

The purpose of the work in this section is to prove the constraint on h in [\(5\)](#)–[\(6\)](#) is sufficient to ensure that if the center column sum S_i is not exact, then it must be exact to $O(h)$. This is the case in which the center column sum is not exact in each of the four standard orientations of the block B_{ij} as shown, for example, in [Figure 3](#). The main result of this section is stated explicitly in [Theorem 3](#) below. Note that it is only necessary to prove this result in one of the four standard orientations of the grid, since the proof of the other three cases is essentially the same. Note also that

in this one case the interface $g(x)$ is monotonically increasing. In Lemma 13 of [23] it is proven if the interface is a nonmonotonically increasing function of x in B_{ij} , then the constraint in (5)–(6) is sufficient to ensure it has two exact column sums, regardless of the manner in which it enters the 3×3 block of cells B_{ij} , passes through the center cell C_{ij} and exits the block B_{ij} again. See Section 3.1 of [23] and, in particular, Lemma 13 for details.

Notation. For convenience, in this section the edges of the 3×3 block of cells B_{ij} will be denoted x_0, x_1, x_2, x_3 , and y_0, y_1, y_2, y_3 , as shown, for example, in Figures 5, 6, and 7. Thus, the 3×3 block B_{ij} will be identified with the 3×3 block $B_{1,1} = [x_0, x_3] \times [y_0, y_3]$ and the center cell C_{ij} will be identified with $C_{1,1} = [x_1, x_2] \times [y_1, y_2]$, the center cell of $B_{1,1}$. Furthermore, in Section 4.1 it will be convenient to translate the coordinate system so the origin $(0, 0)$ coincides with the point (x_0, y_1) . This results in the following relations, which will be used in several of the proofs below: $(x_0, y_1) = (0, 0)$, $(x_1, y_2) = (h, h)$, and $(x_2, y_3) = (2h, 2h)$. For example, see Figure 5.

4.1. The comparison circle $\tilde{z}(s)$. To begin, define the parameters γ and R by

$$\gamma \stackrel{\text{def}}{=} \frac{1}{5} \sqrt{\frac{h\kappa_{\max}}{C_h}}, \quad (20a)$$

$$R \stackrel{\text{def}}{=} 5 \sqrt{\frac{C_h h}{\kappa_{\max}}}, \quad (20b)$$

where C_h is defined in (6), and note that $R\gamma = h$ and, since $0 < h \leq C_h \kappa_{\max}^{-1}$,

$$0 < \gamma \leq \frac{1}{5}. \quad (21)$$

Now consider the *comparison circle* $\tilde{z}(s) = (\tilde{x}(s), \tilde{y}(s))$, which is defined by

$$\tilde{x}(s) = R \sin(\phi_0 + s/R) - R \sin \phi_0, \quad (22a)$$

$$\tilde{y}(s) = -R \cos(\phi_0 + s/R) + R \cos \phi_0, \quad (22b)$$

where ϕ_0 is a parameter defined by

$$\phi_0 = \frac{\pi}{4} - \sin^{-1} \frac{\gamma}{\sqrt{2}}. \quad (23)$$

Note that $\tilde{z}(s) = (\tilde{x}(s), \tilde{y}(s))$ is a circle with radius R , center $(-R \sin \phi_0, R \cos \phi_0)$ and that s is arc length along the circle. In what follows $(x, \tilde{c}(x))$ will sometimes be used to denote the graph of $\tilde{z}(s)$ reparametrized as a function of x , just as $(x, g(x))$ is sometimes used to denote the graph of the interface $z(s)$.

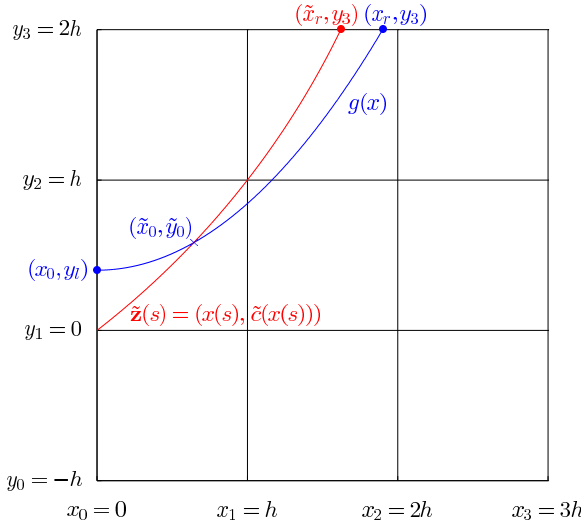


Figure 5. The interface g (shown in blue) is an arbitrary *strictly monotonically increasing* function that enters the 3×3 block B_{ij} through its left edge at the point (x_0, y_l) with $y_1 < y_l < y_2$, passes through the center cell C_{ij} , and exits B_{ij} through the top of its center column S_i at the point (x_r, y_3) , with $x_1 < x_r < x_2$. By [Corollary 2](#) in [Section 4.2](#) if the maximum magnitude κ_{\max} of the curvature κ^g of g satisfies $\kappa_{\max} \leq C_h h^{-1}$, then $x_2 - x_r < \tilde{C} \sqrt{\kappa_{\max}} h^{3/2}$, where the constant \tilde{C} , defined in [\(32\)](#), is independent of h and κ_{\max} . The proof is based on forming a comparison function $\tilde{z}(x) = (x(s), \tilde{c}(x(s)))$ (shown in red), which is a circle that passes through the points $(x_0, y_1) = (0, 0)$ and $(x_1, y_2) = (h, h)$, and proving the abscissa \tilde{x}_r of the point $(\tilde{x}_r, \tilde{c}(\tilde{x}_r)) = (\tilde{x}_r, y_3)$ where \tilde{c} exits the 3×3 block B_{ij} satisfies $x_2 - \tilde{x}_r < \tilde{C} \sqrt{\kappa_{\max}} h^{3/2}$. One then uses [Theorem 2](#) in [Section 4.2](#), the “comparison circle theorem”, to prove the interface g must eventually lie below the graph of \tilde{c} in the open interval (\tilde{x}_0, x_2) . This implies $\tilde{x}_r < x_r$ and hence, $x_2 - \tilde{x}_r < x_2 - x_r < \tilde{C} \sqrt{\kappa_{\max}} h^{3/2}$.

Lemma 1. *Let*

$$s_1 = 2R \sin^{-1} \frac{\gamma}{\sqrt{2}}, \tag{24a}$$

$$s_2 = R \cos^{-1} (\cos \phi_0 - 2\gamma) - R\phi_0, \tag{24b}$$

$$s_3 = R \sin^{-1} (\sin \phi_0 + 2\gamma) - R\phi_0. \tag{24c}$$

Then

$$\tilde{z}(0) = (x_0, y_1) = (0, 0), \tag{25a}$$

$$\tilde{z}(s_1) = (x_1, y_2) = (h, h), \tag{25b}$$

$$\tilde{z}(s_2) = (\tilde{x}(s_2), y_3) = (\tilde{x}_r, 2h), \tag{25c}$$

$$\tilde{z}(s_3) = (x_2, \tilde{y}(s_3)) = (2h, \tilde{y}(s_3)). \tag{25d}$$

The proof is left to the reader.

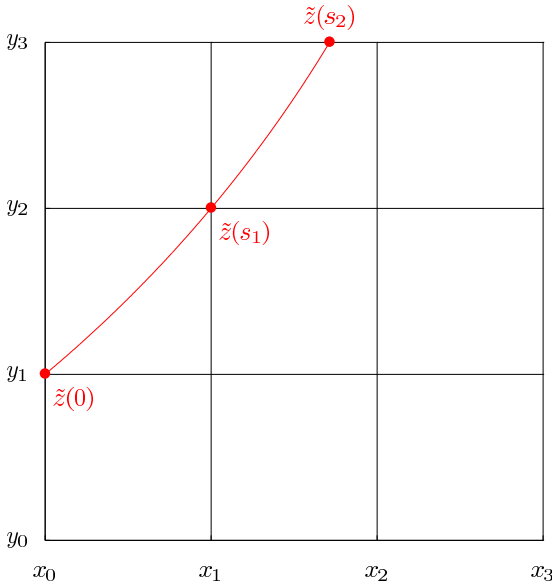


Figure 6. To better visualize the upper and lower bounds on the arc between $\tilde{z}(0) = (0, 0)$ and $\tilde{z}(s_2) = (\tilde{x}(s_2), 2h)$ in [Lemma 4](#), this figure contains an example of the comparison circle $\tilde{z}(s)$ in the 3×3 block $B_{ij} = B_{1,1}$ centered on the cell $C_{ij} = C_{1,1}$.

- Remarks.** (a) In [\(25c\)](#) the variable $\tilde{x}_r = \tilde{x}(s_2)$ is the x -coordinate of the point where the graph of the comparison circle $\tilde{z}(s) = (x, \tilde{c}(x))$ exits the top of the 3×3 block B_{ij} . It plays the same role with respect to the function $\tilde{z}(s)$ as the variable x_r plays with respect to the interface $z(s) = (x, g(x))$. In the problem considered in this section only the case $x_r < x_2 = 2h$ is relevant, for otherwise the center column sum S_i is exact. By [Theorem 2](#) “The Comparison Circle Theorem” below, the interface $(x, g(x))$ must lie below the comparison circle $(x, \tilde{c}(x))$ for $x \geq x_1 = h$ and hence, $x_r < x_2$ implies $\tilde{x}_r < x_2$.
- (b) Note also that [Equation \(25d\)](#) guarantees the comparison circle $(x, \tilde{c}(x))$ must extend all the way to the grid line $x = x_2$, thereby ensuring the comparison circle will lie above the interface $(x, g(x))$ for all $x \in [x_1, x_2]$. This is illustrated in [Figure 7](#).
- (c) Finally, note the comparison circle $\tilde{z}(s)$ is a monotonically increasing function of s for s in the interval $[0, s_3]$ and similarly, when written as a function of x , $(x, \tilde{c}(x))$ is a monotonically increasing function of x for x in the interval $[x_0, x_2] = [0, 2h]$.

The following three lemmas and one corollary concerning the quantities ϕ_0 and s_2 will be needed in the proof that $x_2 - \tilde{x}_r$ is $O(\sqrt{\kappa_{\max}}h^{3/2})$ and hence, $x_2 - x_r$ is also $O(\sqrt{\kappa_{\max}}h^{3/2})$.

Lemma 2. $(\cos \phi_0 - \sin \phi_0 = \gamma)$ Let ϕ_0 be defined as in (23):

$$\phi_0 = \frac{\pi}{4} - \sin^{-1} \frac{\gamma}{\sqrt{2}}.$$

Then

$$\cos \phi_0 - \sin \phi_0 = \gamma. \tag{26}$$

Proof. Define β by

$$\sin \beta \stackrel{\text{def}}{=} \frac{\gamma}{\sqrt{2}}$$

so that

$$\phi_0 = \frac{\pi}{4} - \sin^{-1} \frac{\gamma}{\sqrt{2}} = \frac{\pi}{4} - \beta.$$

Then (26) follows from writing ϕ_0 as $\pi/4 - \beta$ and applying the trigonometric identities for the sine and cosine of the difference of two angles:

$$\cos \phi_0 - \sin \phi_0 = \sqrt{2} \sin \beta = \gamma. \quad \square$$

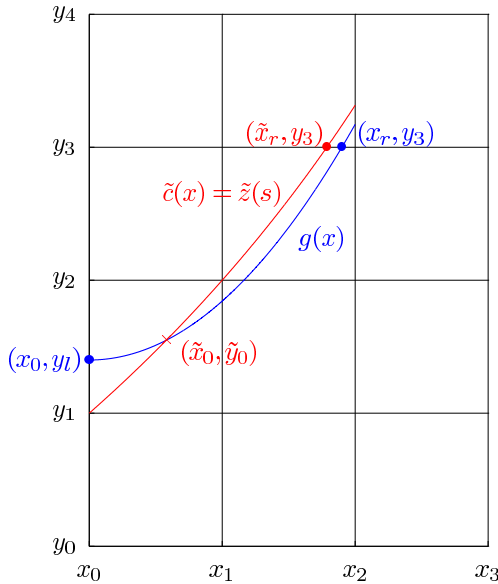


Figure 7. This figure includes the row of cells that lie above the standard 3×3 block of cells $B_{ij} = B_{1,1}$ centered on $C_{ij} = C_{1,1} = [x_1, x_2] \times [y_1, y_2]$ in which the approximation to the monotonically increasing interface g , shown in blue, will be constructed. The difference between the center column sum S_i and the exact volume (i.e., exact area) in B_{ij} under $g(x)$ is the region in the center column that lies under the graph of g and above the line $y = y_3$. By **Theorem 2** the comparison circle $\tilde{c}(x)$, shown in red, bounds $g(x)$ from above for all $x \in [\tilde{x}_0, \tilde{x}_2]$, and hence, allows one to bound the difference between S_i and the integral of $g(x) - y_0$ over $[x_1, x_2]$.

Lemma 3. ($\cos \phi_0 + \sin \phi_0 = \sqrt{2 - \gamma^2}$) Let ϕ_0 be defined as in (23). Then

$$\cos \phi_0 + \sin \phi_0 = \sqrt{2 - \gamma^2}. \quad (27)$$

Proof. As in the proof of the previous lemma let β be defined by $\sin \beta = \gamma / \sqrt{2}$. Then (27) is a consequence of the trigonometric identities for the sine and cosine of the difference of two angles, together with the trigonometric identity

$$\cos(\arcsin(x)) = \sqrt{1 - x^2},$$

as follows:

$$\cos \phi_0 + \sin \phi_0 = \sqrt{2} \cos \beta = \sqrt{2} \cos \left(\sin^{-1} \frac{\gamma}{\sqrt{2}} \right) = \sqrt{2 - \gamma^2}. \quad \square$$

Lemma 4. ($s_2 = O(h)$) Let s_2 be the parameter defined in (24b). Then s_2 satisfies

$$(1 + \sqrt{2})h < s_2 < 4h. \quad (28)$$

Proof. Recall that s is arc length along the comparison circle $\tilde{z}(s) = (\tilde{x}(s), \tilde{y}(s))$ starting at the point $\tilde{z}(0) = (\tilde{x}(0), \tilde{y}(0)) = (x_0, y_1) = (0, 0)$. The length of the arc of the comparison circle from $\tilde{z}(0)$ to $\tilde{z}(s_2)$ consists of two sections. The first section is the arc from $\tilde{z}(0)$ to $\tilde{z}(s_1) = (x_1, y_2) = (h, h)$ while the second section is the arc from $\tilde{z}(s_1)$ to $\tilde{z}(s_2) = (\tilde{x}(s_2), y_3) = (\tilde{x}_r, y_3)$.

The length of the first section is bounded below by the length of the diagonal joining $(0, 0)$ and (h, h) , which has length $\sqrt{2}h$, and is bounded above by the sum of the lengths of the bottom and right edges of the cell that has $(0, 0)$ and (h, h) as its opposite corners; i.e., the edge connecting $(0, 0) = (x_0, y_1)$ and the corner (x_1, y_1) and the edge connecting (x_1, y_1) and the corner $(h, h) = (x_1, y_2)$. Since both of these edges have length h , it follows that the portion of the arc joining $\tilde{z}(0)$ to $\tilde{z}(s_1)$ is bounded above by $2h$.

Since the point $\tilde{z}(s_2)$ lies on the top edge of the 3×3 block B_{ij} and, since $\tilde{z}(s)$ is a monotonically increasing function of s for $0 \leq s \leq s_3$, $\tilde{x}(s_2) = \tilde{x}_2$ must lie between x_1 and x_2 . It follows that a lower bound for the portion of the arc joining $\tilde{z}(s_1)$ to $\tilde{z}(s_2)$ is the length of the side of the cell joining the point $(h, h) = (x_1, y_2)$ and the point (x_1, y_3) on the top edge of $B_{ij} = B_{1,1}$. Since this edge has length h , it follows that a lower bound for the length of the arc joining $\tilde{z}(0)$ to $\tilde{z}(s_2)$, and hence a lower bound for s_2 , is $\sqrt{2}h + h = (\sqrt{2} + 1)h$ as shown in the inequality on the left in (28).

One can find an upper bound for the portion of the arc joining $\tilde{z}(s_1)$ to $\tilde{z}(s_2)$ by using reasoning that is identical to that used to obtain the upper bound on the portion of the arc joining $\tilde{z}(0)$ to $\tilde{z}(s_1)$. This yields an upper bound of $2h + 2h = 4h$ for the entire length of the arc joining $\tilde{z}(0)$ to $\tilde{z}(s_2)$, as shown in the inequality on the right in (28). \square

The proof of the next theorem depends on the following corollary.

Corollary 1. (θ is $O(\gamma)$) Let s_2 be the parameter defined in (24b) and define θ by

$$\theta \stackrel{\text{def}}{=} \frac{s_2}{R}. \quad (29)$$

Then θ satisfies

$$(1 + \sqrt{2})\gamma < \theta < 4\gamma. \quad (30)$$

Proof. One obtains the inequality in (30) by multiplying Equation (28) in Lemma 4 by R^{-1} and recalling that $h = R\gamma$. \square

The following theorem is the key step in the proof that $|x_2 - x_r| = O(\sqrt{\kappa_{\max}} h^{3/2})$.

Theorem 1 ($x_2 - \tilde{x}_r < \tilde{C} \sqrt{\kappa_{\max}} h^{3/2}$). The difference $x_2 - \tilde{x}_r$ is bounded above by

$$x_2 - \tilde{x}_r < \tilde{C} \sqrt{\kappa_{\max}} h^{3/2}, \quad (31)$$

where $\tilde{x}_r = \tilde{x}(s_2)$ is defined in (25c) and

$$\tilde{C} \stackrel{\text{def}}{=} \frac{2\sqrt{66}}{3 \cdot 5^4} \{736\sqrt{2} - 349\} \approx 5.995421. \quad (32)$$

Remark 1. (a) One of the consequences of replacing the Lemmas, Theorems, and Corollaries in Sections 3.2–3.4 of [23] with those in Section 4 here is that the term bounding the difference $x_2 - \tilde{x}_r$ in (31) above now depends linearly on $\sqrt{\kappa_{\max}}$. As a result, the term on the right-hand side of (12) and (52) depends linearly on κ_{\max} , which in turn leads to a linear dependence of the bounds in (13) and (58) on κ_{\max} . The analogous bounds in Theorems 15, 23, and 25 of [23] do not depend linearly on κ_{\max} .

(b) As mentioned in Remark 1(a), it is possible that $\tilde{x}_r \geq x_2$. In this case, by the comparison circle theorem below, $x_r > x_2$ and hence, the center column sum S_i must be exact. Since the purpose of this section is to prove S_i must be exact to $O(h)$ if g satisfies (5)–(6) and S_i is not exact, the case in which S_i is exact, or equivalently, $\tilde{x}_r \geq x_2$, is not of interest here.

Proof. Since the coordinate system has been arranged so the origin $(0, 0)$ coincides with the point (x_0, y_1) and hence, $x_2 = 2h = y_3$ (e.g., see Figure 5), it follows that

$$x_2 = 2h = \tilde{y}(s_2).$$

Thus

$$\begin{aligned} x_2 - \tilde{x}_r &= \tilde{y}(s_2) - \tilde{x}(s_2) \\ &= R\{(\cos \phi_0 - \cos(\phi_0 + s_2/R)) - (-\sin \phi_0 + \sin(\phi_0 + s_2/R))\}. \end{aligned} \quad (33)$$

Since $R = 5\sqrt{C_h h / \kappa_{\max}}$, it suffices to show that the quantity inside the curly braces in (33) is $O(\gamma^2) = O(h\kappa_{\max}/C_h)$. One can rewrite (33) as

$$x_2 - \tilde{x}_r = R\{(\cos \phi_0 + \sin \phi_0) - (\cos(\phi_0 + \theta) + \sin(\phi_0 + \theta))\} = RA, \quad (34)$$

where $\theta = s_2/R$ was defined in Corollary 1 above. Consider the quantity A obtained by dividing (34) by R ,

$$A = \{(\cos \phi_0 + \sin \phi_0) - (\cos(\phi_0 + \theta) + \sin(\phi_0 + \theta))\}. \quad (35)$$

Now expand $\cos(\phi_0 + \theta)$ and $\sin(\phi_0 + \theta)$ in a Taylor series about $\cos \phi_0$ and $\sin \phi_0$, respectively, to obtain

$$\begin{aligned} A &= (\cos \phi_0 + \sin \phi_0) - (\cos(\phi_0 + \theta) + \sin(\phi_0 + \theta)) \\ &= -(\cos \phi_0 - \sin \phi_0)\theta + (\cos \phi_0 + \sin \phi_0)\frac{\theta^2}{2!} \\ &\quad + (\cos \phi_0 - \sin \phi_0)\frac{\theta^3}{3!} - (\cos \phi_0 + \sin \phi_0)\frac{\theta^4}{4!} \\ &\quad - (\cos \phi_0 - \sin \phi_0)\frac{\theta^5}{5!} + (\cos \phi_0 + \sin \phi_0)\frac{\theta^6}{6!} \\ &\quad + (\cos \phi_0 - \sin \phi_0)\frac{\theta^7}{7!} - (\cos \phi_0 + \sin \phi_0)\frac{\theta^8}{8!} + \dots \end{aligned}$$

This expression for A can be rewritten as

$$\begin{aligned} A &= -\left((\cos \phi_0 - \sin \phi_0) - (\cos \phi_0 + \sin \phi_0)\frac{\theta}{2}\right)\theta \\ &\quad + \left((\cos \phi_0 - \sin \phi_0) - (\cos \phi_0 + \sin \phi_0)\frac{\theta}{4}\right)\frac{\theta^3}{3!} \\ &\quad - \left((\cos \phi_0 - \sin \phi_0) - (\cos \phi_0 + \sin \phi_0)\frac{\theta}{6}\right)\frac{\theta^5}{5!} \\ &\quad + \left((\cos \phi_0 - \sin \phi_0) - (\cos \phi_0 + \sin \phi_0)\frac{\theta}{8}\right)\frac{\theta^7}{7!} + \dots \end{aligned} \quad (36)$$

Using Lemmas 2 and 3 one can rewrite this series in terms of θ and γ as

$$\begin{aligned} A &= -\left(\gamma - \frac{\theta}{2}\sqrt{2-\gamma^2}\right)\theta + \left(\gamma - \frac{\theta}{4}\sqrt{2-\gamma^2}\right)\frac{\theta^3}{3!} \\ &\quad - \left(\gamma - \frac{\theta}{6}\sqrt{2-\gamma^2}\right)\frac{\theta^5}{5!} + \left(\gamma - \frac{\theta}{8}\sqrt{2-\gamma^2}\right)\frac{\theta^7}{7!} - \dots \end{aligned} \quad (37)$$

The first term, A_1 , in this series is $O(\gamma^2)$. To see this note that the upper bound on θ in (30) implies

$$A_1 = \left(\frac{\theta}{2}\sqrt{2-\gamma^2} - \gamma\right)\theta < (2\sqrt{2}-1)4\gamma^2, \quad (38)$$

where the upper bound on $\sqrt{2-\gamma^2}$ follows from $0 < \gamma \leq 1/5$ in (21). Furthermore, $A_1 > 0$. To see this first note that since θ is always positive the sign of A_1 depends only on the terms in parentheses on the right-hand side of the equal sign in (38). Since $\theta > (1 + \sqrt{2})\gamma > 0$ by (30),

$$\begin{aligned} \frac{A_1}{\theta} &= \left(\frac{\theta}{2} \sqrt{2-\gamma^2} - \gamma \right) > \left(\frac{(1 + \sqrt{2})}{2} \sqrt{2 - \frac{1}{25}} - 1 \right) \gamma \\ &= \left(\frac{7(1 + \sqrt{2})}{10} - 1 \right) \gamma > 0, \end{aligned} \tag{39}$$

where the lower bound on $\sqrt{2-\gamma^2} > \sqrt{2-25^{-1}}$ also follows from (21).

In order to obtain an absolute upper bound on the entire series A in (37), and thus on $x_2 - \tilde{x}_r = RA$, begin by writing A in the form

$$A = A_1 + A_2 - B,$$

where

$$A_2 = \left(\gamma - \frac{\theta}{4} \sqrt{2-\gamma^2} \right) \frac{\theta^3}{3!},$$

and B is an alternating series of the form

$$B = b_1 - b_2 + b_3 - \dots ,$$

with the j -th term b_j of this series given by

$$b_j = \left(\gamma - \frac{\theta}{2j+4} \sqrt{2-\gamma^2} \right) \frac{\theta^{(2j+3)}}{(2j+3)!} \quad \text{for } j = 1, 2, 3, \dots \tag{40}$$

Using the same techniques one uses to derive the upper and lower bounds on A_1 in (38) and (39), respectively, one can derive the following upper and lower bounds for A_2 ,

$$\begin{aligned} (1 - \sqrt{2}) \frac{(1 + \sqrt{2})^3}{6} \gamma^4 &< A_2 = \left(\gamma - \frac{\theta}{4} \sqrt{2-\gamma^2} \right) \frac{\theta^3}{3!} \\ &< \left(1 - \frac{7(1 + \sqrt{2})}{20} \right) \frac{32}{3} \gamma^4. \end{aligned} \tag{41}$$

It is apparent from the bounds in (41) that A_2 may be either positive or negative, depending on the values of h and κ_{\max} .

Now note that each of the terms b_j defined in (40) of the series B are positive. To see this, first note that, since θ is positive by (30), the sign of b_j depends only on the terms in parentheses immediately to the right of the equal sign in (40). For

example,

$$b_1 = \left(\gamma - \frac{\theta}{6} \sqrt{2 - \gamma^2} \right) \frac{\theta^5}{5!} > 0,$$

since $0 < \gamma \leq 1/5$, $0 < \theta < 4\gamma$ and $\sqrt{2 - \gamma^2} < \sqrt{2}$, and hence,

$$\left(\gamma - \frac{\theta}{6} \sqrt{2 - \gamma^2} \right) > \left(1 - \frac{2}{3} \sqrt{2} \right) \gamma > 0. \quad (42)$$

Similarly, all of the subsequent terms in this series are also positive, since (42) implies the terms in parentheses immediately to the right of the equal sign in the definition of b_j for $j > 1$ in (40) must also be positive,

$$\left(\gamma - \frac{\theta}{2j+4} \sqrt{2 - \gamma^2} \right) > \left(\gamma - \frac{\theta}{6} \sqrt{2 - \gamma^2} \right) > 0 \quad \text{for all } j = 2, 3, 4, \dots$$

Furthermore, it is also the case that $b_j > b_{j+1}$ for all $j = 1, 2, 3, \dots$, since the terms b_j defined in (40) are (strictly) monotonically decreasing when viewed as a function of j . (To see this recall $\gamma \leq 1/5$ from (21) and hence, (30) implies $\theta < 4\gamma \leq 4/5$.) Finally, since $b_j > 0$ and $b_j > b_{j+1}$ for all $j = 1, 2, 3, \dots$, it follows that the entire series B is positive,

$$B = (b_1 - b_2) + (b_3 - b_4) + (b_5 - b_6) + \dots > 0.$$

This leads to an absolute upper bound on the series A in (37),

$$A = A_1 + A_2 - B < A_1 + A_2 < (2\sqrt{2} - 1)4\gamma^2 + \left(1 - \frac{7(1 + \sqrt{2})}{20} \right) \frac{32}{3} \gamma^4. \quad (43)$$

Finally, since $\gamma = \sqrt{h\kappa_{\max}}/5\sqrt{C_h}$, $R\gamma = h$ and, by (21), $\gamma^2 \leq 1/25$, the upper bound on $x_2 - \tilde{x}_r$ in (31) now follows from (34) and (43),

$$\begin{aligned} x_2 - \tilde{x}_r &= RA \leq R \left\{ (2\sqrt{2} - 1)4\gamma^2 + \left(1 - \frac{7(1 + \sqrt{2})}{20} \right) \frac{32}{3} \gamma^4 \right\} \\ &\leq \frac{\sqrt{33}}{5\sqrt{2}} \left\{ 8\sqrt{2} - 4 + \frac{8}{3 \cdot 25} \left(\frac{13}{5} - \frac{7\sqrt{2}}{5} \right) \right\} \sqrt{\kappa_{\max}} h^{3/2} \\ &= \tilde{C} \sqrt{\kappa_{\max}} h^{3/2}. \quad \square \end{aligned}$$

4.2. The comparison circle theorem. Suppose the interface $(x, g(x))$ satisfies $h \leq C_h \kappa_{\max}^{-1}$ and $x_r < x_2$ where (x_r, y_3) is the point at which g exits the 3×3 block of cells B_{ij} . The following theorem states that once $g(x) < \tilde{c}(x)$ for some $x \in (x_0, x_2)$, then $g(x)$ must remain below $\tilde{c}(x)$ for all $x \in (\tilde{x}_0, x_2)$, where $(\tilde{x}_0, \tilde{y}_0)$ denotes the point where g initially crosses below \tilde{c} as illustrated in Figures 5 and 7. An immediate consequence of this theorem is $\tilde{x}_r < x_r$. Consequently, if

$x_r < x_2$, then $\tilde{x}_r < x_r < x_2$ and hence, $x_2 - x_r < x_2 - \tilde{x}_r$. Since by [Theorem 1](#), $x_2 - \tilde{x}_r < \tilde{C} \sqrt{\kappa_{\max}} h^{3/2}$, it follows that $x_2 - x_r < \tilde{C} \sqrt{\kappa_{\max}} h^{3/2}$. This, together with the bound on $|g'(x)|$ in [\(A.5a\)](#), is sufficient to ensure the error in the center column sum S_i associated with g is $O(h)$.

Theorem 2 (the comparison circle theorem). *Let R as defined in [\(20b\)](#) be the radius of the comparison circle [\(22\)](#) and let $g \in C^2[x_0, x_2]$ be a strictly monotonic function that satisfies [\(5\)](#), where the constant C_h is defined in [\(6\)](#). Furthermore, assume the interface g enters the 3×3 block of cells B_{ij} across its left edge at the point (x_0, y_1) with $y_1 < y_l < y_2$, passes through the center cell C_{ij} , and exits B_{ij} through the top of its center column at the point (x_r, y_3) with $x_1 < x_r < x_2$. Let $(\tilde{x}_0, \tilde{y}_0)$ denote the first point at which the graph of g crosses the graph of \tilde{c} as shown, for example, in [Figures 5 and 7](#). Then*

$$g(x) < \tilde{c}(x) \quad \text{for all } x \in (\tilde{x}_0, x_r]. \tag{44}$$

Proof. First note that, since the interface g satisfies [\(5\)](#) where C_h is defined by [\(6\)](#), this ensures the maximum curvature κ_{\max} of g is bounded above by the curvature $\kappa^{\tilde{c}}$ of the comparison circle,

$$\kappa_{\max} < R^{-1} = \kappa^{\tilde{c}}.$$

The argument is as follows. Since the interface satisfies [\(5\)](#)–[\(6\)](#), it follows that $\kappa_{\max} \leq C_h h^{-1}$ and hence,

$$\sqrt{\kappa_{\max}} \leq \sqrt{\frac{C_h}{h}}. \tag{45}$$

Multiplying both sides of [\(45\)](#) by $\sqrt{\kappa_{\max}}$ yields

$$\kappa_{\max} \leq \sqrt{\frac{C_h \kappa_{\max}}{h}}. \tag{46}$$

Now, since $(5C_h)^{-1} = 3.3 > 1$, we can bound the right-hand side of [\(46\)](#) by

$$\kappa_{\max} \leq \sqrt{\frac{C_h \kappa_{\max}}{h}} < \frac{1}{5C_h} \sqrt{\frac{C_h \kappa_{\max}}{h}} \leq \frac{1}{5} \sqrt{\frac{\kappa_{\max}}{C_h h}} = R^{-1} = \kappa^{\tilde{c}}.$$

Thus, κ_{\max} , the maximum magnitude of the curvature of g , is bounded above by the curvature $\kappa^{\tilde{c}} = R^{-1}$ of the comparison circle and therefore,

$$\kappa^g(x) \leq \kappa_{\max} < \kappa^{\tilde{c}}(x) = R^{-1} \quad \text{for all } x \in [x_0, x_2]. \tag{47}$$

The inequality in [\(44\)](#) is proven by contradiction. One begins by assuming

$$g(\xi) = \tilde{c}(\xi) \quad \text{for some } \xi \in (\tilde{x}_0, x_r], \tag{48}$$

and then showing that this implies the maximum curvature κ_{\max} of g in (\tilde{x}_0, x_r) must exceed $\kappa^{\tilde{c}}$, thereby contradicting (47). The argument is as follows. Let ξ denote the first point in $(\tilde{x}_0, x_r]$ that satisfies (48). Since $g(x) > \tilde{c}(x)$ for $x_0 < x < \tilde{x}_0$ and $g(x) < \tilde{c}(x)$ for $\tilde{x}_0 < x < \xi$, it follows that

$$g'(\tilde{x}_0) < \tilde{c}'(\tilde{x}_0), \quad (49)$$

However, since, by assumption, $g(\xi) = \tilde{c}(\xi)$ for some $\xi > \tilde{x}_0$ (i.e., (48) holds), it must be the case that eventually $g'(x) \geq \tilde{c}'(x)$. Let $x^* \in (\tilde{x}_0, \xi)$ be the first x such that $g'(x^*) = \tilde{c}'(x^*)$ so that

$$g'(x^*) = g'(\tilde{x}_0) + \int_{\tilde{x}_0}^{x^*} g''(x) dx = \tilde{c}'(\tilde{x}_0) + \int_{\tilde{x}_0}^{x^*} \tilde{c}''(x) dx = \tilde{c}'(x^*).$$

By virtue of (49) this can only be true if $g''(x) > \tilde{c}''(x)$ on some subinterval of (\tilde{x}_0, x^*) . In particular,

$$g''(\eta) > \tilde{c}''(\eta), \quad (50)$$

for some $\eta \in (\tilde{x}_0, x^*)$.

Now recall the following three facts.

- (1) By assumption g is strictly monotonic and hence, $0 < g'(x)$ for all $x \in (x_0, \tilde{x}_r]$.
- (2) For all $x \in (\tilde{x}_0, x^*)$, $0 < g'(x) < \tilde{c}'(x)$.
- (3) For all $x \in [x_0, x_2]$, $\kappa^g(x) = g''(x)(\sqrt{1 + g'(x)^2})^{-3}$ (e.g., see [29]).

Equation (50) together with items (1)-(3) above imply

$$\kappa^g(\eta) = \frac{g''(\eta)}{(\sqrt{1 + g'(\eta)^2})^3} > \frac{\tilde{c}''(\eta)}{(\sqrt{1 + \tilde{c}'(\eta)^2})^3} = \kappa^{\tilde{c}}(\eta),$$

which contradicts (47). Therefore, g must be bounded above by the comparison circle as claimed. \square

Corollary 2 ($x_2 - x_r < \tilde{C} \sqrt{\kappa_{\max} h^{3/2}}$). *Let $g \in C^2[x_0, x_3]$ be a function that satisfies the assumptions stated in Theorem 2. Then*

$$x_2 - x_r < \tilde{C} \sqrt{\kappa_{\max} h^{3/2}}, \quad (51)$$

where \tilde{C} is defined in (32).

Proof. By the Comparison Circle Theorem (Theorem 2) there exists a point $\tilde{x}_0 \in (x_0, x_r)$ such that

$$g(x) < \tilde{c}(x) \quad \text{for all } x \in (\tilde{x}_0, x_r).$$

This implies $\tilde{x}_r < x_r$, and hence that $x_2 - x_r < x_2 - \tilde{x}_r$. Equation (51) follows immediately from (31) in Theorem 1. \square

4.3. The column sum S_i is exact to $O(h)$.

Theorem 3 (the column sum S_i is exact to $O(h)$). *Assume the interface $g \in C^2[x_0, x_3]$ and g is a strictly monotonically increasing function that satisfies the constraint in (5) with the constant C_h defined in (6). Furthermore, assume g enters the 3×3 block of cells $B_{ij} = B_{11} = [x_0, x_3] \times [y_0, y_3]$ across its left edge at the point (x_0, y_l) with $y_1 < y_l < y_2$, passes through the center cell $C_{ij} = C_{11} = [x_1, x_2] \times [y_1, y_2]$, and exits B_{ij} through the top of its center column at the point (x_r, y_3) with $x_1 < x_r < x_2$ as shown, for example, in Figure 7. Then the error between the normalized integral of g over the center column and the column sum S_i is $O(h)$:*

$$\left| \frac{1}{h^2} \int_{x_1}^{x_2} (g(x) - y_0) dx - S_i \right| < \bar{C} \kappa_{\max} h, \quad (52)$$

where

$$\bar{C} \stackrel{\text{def}}{=} \tilde{C}^2, \quad (53)$$

and \tilde{C} is defined in (32).

Proof. Since, by assumption,

$$\min_{[x_0, x_r]} g(x) = y_l > y_1 > y_0,$$

and the interface is a strictly monotonically increasing function of x on $[x_0, x_2]$, it follows that

$$S_i = h^{-2} \int_{x_1}^{x_2} (\min\{g(x), y_3\} - y_0) dx.$$

The error between the normalized volume (i.e., area) under the interface $y = g(x)$ in the center column and the center column sum S_i is therefore

$$h^{-2} \int_{x_1}^{x_2} (g(x) - y_0) dx - S_i = h^{-2} \int_{x_r}^{x_2} (g(x) - y_3) dx. \quad (54)$$

An example is shown in Figure 7. Thus, it suffices to show

$$\left| \int_{x_r}^{x_2} (g(x) - y_3) dx \right| \leq \bar{C} \kappa_{\max} h^3. \quad (55)$$

By (A.5a) $|g'(x)| < 2$, which implies

$$\left| \int_{x_r}^{x_2} (g(x) - y_3) dx \right| \leq \left| \int_{x_r}^{x_2} L(x) dx \right|, \quad (56)$$

where $L(x)$ is the line with slope 2 that passes through the point x_r . The region of integration on the right hand side of (56) is a right triangle with corners (x_r, y_3) ,

(x_2, y_3) , and $(x_2, y_3 + 2(x_2 - x_r))$, and hence the integral on the right-hand side of (56) is the area of this triangle, namely $(x_2 - x_r)^2$. Thus,

$$\left| \int_{x_r}^{x_2} (g(x) - y_3) dx \right| \leq \left| \int_{x_r}^{x_2} L(x) dx \right| \leq (x_2 - x_r)^2 < \tilde{C}^2 \kappa_{\max} h^3 = \bar{C} \kappa_{\max} h^3, \quad (57)$$

where the bound $(x_2 - x_r)^2 < \tilde{C}^2 \kappa_{\max} h^3$ between the third and fourth terms in (57) follows from Equation (51) in Corollary 2. Equation (52), and hence the theorem, now follows immediately from (54) and (57). \square

5. Second-order accuracy in the max norm

All of the results in Section 4 (“Second-order accuracy in the max norm”) of [23] now hold provided the interface is a C^2 simple closed curve, the constraint in (5)–(6) is satisfied, the constant C_S in the statement of Theorem 23 in [23] is replaced by the constant \bar{C} defined in (53), and the term $(50\kappa_{\max}/3 + C_S)$ that appears in the statement of Theorem 24 of [23] is replaced by $C_m \kappa_{\max}$, where the constant C_m is defined in (59) below.

The key theorem that has changed between the two papers is Theorem 15 of [23]. Theorem 3 above is a stronger version of this theorem. Theorem 3 ensures that in cases such as the one shown in Figure 3, if the interface is C^2 and the constraint in (5)–(6) is satisfied, then in some orientation of the 3×3 block of cells B_{ij} centered on the cell C_{ij} in which one wishes to reconstruct the interface, there is a parametrization of the interface of the form $y = g(x)$ or $x = G(y)$, such that the center column sum S_i in the new orientation of the 3×3 block is exact to $O(h)$. This result provides the basis for the main result of this article, namely Theorem 4 below, which is a stronger version of Theorem 24, the main result of [23]. As has been the case throughout this article, in the statement of Theorem 4 below the interface $\tilde{z}(s)$ is written in the form $y = g(x)$ with material 1 lying below the graph of g , with the understanding the theorem also holds in those cases in which one must instead express the interface in the form $x = G(y)$ with material 1 lying below the graph of G .

Theorem 4. *Assume the interface $g \in C^2[x_{i-1}, x_{i+2}]$ and the grid size h and the maximum magnitude of the curvature κ_{\max} of the interface in the 3×3 block of cells B_{ij} centered on the cell C_{ij} in which one wishes to reconstruct the interface satisfy*

$$h \leq C_h \kappa_{\max}^{-1} = \frac{2}{33} \kappa_{\max}^{-1}. \quad (5)$$

Then there exists $\alpha, \beta = 1, 0, -1$ with $\alpha \neq \beta$ such that the column sums $S_{i+\alpha}$ and $S_{i+\beta}$ in B_{ij} are either exact or exact to $O(h)$. Furthermore, let

$$\tilde{g}_{ij}(x) = m_{ij}x + b_{ij}$$

be a piecewise linear approximation to $g(x)$ for $x \in [x_i, x_{i+1}]$ such that $g(x)$ and $\tilde{g}_{ij}(x)$ have the same volume fraction in the center cell

$$\Lambda_{ij}(g) = \Lambda_{ij}(\tilde{g}) \quad \text{and} \quad m_{ij} = \frac{(S_{i+\alpha} - S_{i+\beta})}{(\alpha - \beta)}.$$

Then $\tilde{g}_{ij}(x)$ is a pointwise, second-order accurate approximation to $g(x)$ in the interval $[x_i, x_{i+1}]$,

$$|g(x) - \tilde{g}_{ij}(x)| \leq \frac{25}{12}\kappa_{\max}h^2 + \bar{C}\kappa_{\max}h^2 = C_m\kappa_{\max}h^2 \quad \text{for all } x \in [x_i, x_{i+1}], \quad (58)$$

where

$$C_m \stackrel{\text{def}}{=} \left\{ \frac{25}{12} + \bar{C} \right\}, \quad (59)$$

and the constant \bar{C} is defined in (53).

Proof. The proof of this theorem is identical to the proof of Theorem 24 in [23] after one replaces the constant C_S defined in equation (89) of [23] with $\bar{C}\kappa_{\max}$, where \bar{C} is defined in (53) above. \square

6. Conclusions

This article contains a proof of the following result. Suppose one is given a square grid with cells of side h covering a closed and bounded rectangle $\Omega \subset \mathbb{R}^2$ and a C^2 simple closed curve $z(s)$ in Ω . If

$$h \leq C_h(\kappa_{\max})^{-1} = \frac{2}{33}(\kappa_{\max})^{-1}, \quad (5)$$

where κ_{\max} is the maximum magnitude of the curvature $\kappa(s)$ of the interface z in Ω . Then in every cell $C_{ij} = [x_i, x_{i+1}] \times [y_j, y_{j+1}]$ that contains a portion of the interface there exists a piecewise linear function $\tilde{g}_{ij}(x) = m_{ij}x + b_{ij}$ that is a second-order accurate approximation to the portion of the interface $y = g(x)$ that lies in C_{ij} ,

$$|g(x) - \tilde{g}_{ij}(x)| \leq C_m\kappa_{\max}h^2 \quad \text{for all } x \in [x_i, x_{i+1}],$$

where C_m is a constant, defined in (59) above, which is independent of h and κ_{\max} . For convenience, the interface $z(s)$ has been written here as a function $y = g(x)$ of the independent variable x with it being understood that in some cells it may be necessary to express the interface as a function $x = G(y)$ of the independent variable y . Theorem A.1 in the Appendix ensures if h satisfies the constraint in (5)–(6), then the interface can be written as a single-valued function of at least one of the coordinate variables x or y in every 3×3 block of cells centered on every cell C_{ij} that contains a portion of the interface.

In an earlier paper [23] the author proved a similar result, but with a constraint on the cell size h that was more restrictive than the one in (5)–(6). In order to obtain the less restrictive constraint on h in (5)–(6) Sections 3.2–3.4 of [23] required extensive modification. These modifications constitute Section 4 of the present paper.

The algorithm described in [24] is an example of a volume-of-fluid interface reconstruction algorithm that satisfies conditions (I)–(V) on page 125 of this article and hence, by Theorem 4 above, produces a pointwise second-order accurate approximation to the interface $\mathbf{z}(s)$.

Future work in this area should include the analysis of fingers and other regions of large curvature in both stationary and moving interfaces in an effort to determine conditions such as (5)–(6) that will ensure all filaments and similar regions are accurately resolved on grids that satisfy these conditions. Future work should also include proving the volume-of-fluid interface reconstruction algorithm coupled to a volume-of-fluid advection algorithm produces a second-order accurate approximation to the solutions of the advection equation.

Appendix: Considerations that affect the value of C_h

Definition. Let $a > 2$ be a real-valued parameter and define $\bar{C}_h[a]$ by

$$\bar{C}_h[a] \stackrel{\text{def}}{=} \frac{\sqrt{a} - \sqrt{2}}{4\sqrt{2}\sqrt{a-1}}. \quad (\text{A.1})$$

The following theorem is a generalization of Theorem 6 of [23].

Theorem A.1. For $s_L \leq s \leq s_R$ with $\mathbf{z}(s_L) = \mathbf{z}(s_R)$ let s be arclength along the two times continuously differentiable simple closed curve $\mathbf{z}(s)$ in Ω . Given some $s_0 \in [s_L, s_R]$ such that

$$\dot{\mathbf{y}}^2(s_0) \leq \frac{1}{2} \leq \dot{\mathbf{x}}^2(s_0), \quad (\text{A.2})$$

suppose one wants to reconstruct the interface in a neighborhood of the point $\mathbf{z}(s_0) = (x(s_0), y(s_0))$. Let $a > 2$ be a real-valued parameter as in (A.1) above and let $s_l \geq s_L$ be the greatest number less than s_0 and $s_r \leq s_R$ be the smallest number greater than s_0 such that

$$\dot{\mathbf{x}}^2(s_l) = \frac{1}{a} = \dot{\mathbf{x}}^2(s_r), \quad (\text{A.3})$$

so $a^{-1} \leq \dot{\mathbf{x}}^2(s) \leq 1$ for all $s \in [s_l, s_r]$. Let $x_0 = x(s_0)$ and let

$$h_{\max} \stackrel{\text{def}}{=} \bar{C}_h[a] \kappa_{\max}^{-1} \quad (\text{A.4})$$

where $\bar{C}_h[a]$ is defined in (A.1) above. Then one can represent the interface as a single-valued function $y = g(x)$ of x on the interval

$$[x_l, x_r] = [x_0 - 2h_{\max}, x_0 + 2h_{\max}].$$

In addition, for all $x \in [x_l, x_r]$,

$$\max_{x \in [x_l, x_r]} |g'(x)| \leq \sqrt{a-1}, \tag{A.5a}$$

$$\max_{x \in [x_l, x_r]} |g''(x)| \leq (\sqrt{a})^3 \kappa_{\max}. \tag{A.5b}$$

Furthermore, if the roles of \dot{x} and \dot{y} in (A.2) and (A.3) are reversed, then one can represent the interface as a single-valued function $x = G(y)$ of y on the interval $[y_l, y_r] = [y_0 - 2h_{\max}, y_0 + 2h_{\max}]$ and the bounds in (A.5) hold on the interval $[y_l, y_r]$ with the function $g(x)$ replaced by $G(y)$.

Proof. Let $a > 2$ be the parameter in the definition of $\bar{C}_h[a]$ in (A.1) above. The proof of this theorem is identical to the proof of Lemmas 3–5 and Theorem 6 in [23] after one replaces the constants $1/4$ and $3/4$ in equation (23) in Lemma 3 of [23] with $1/a$ and $(a-1)/a$, respectively, and makes similar substitutions in Lemmas 4–5 and Theorem 6 of the same. \square

Remarks. (1) Theorem 6 of [23] is the special case of Theorem A.1 with $a = 4$.

(2) If necessary, one can periodically extend the interval $[x_L, x_R] \stackrel{\text{def}}{=} [x(s_L), x(s_R)]$ to the interval $[x_L - D, x_R + D]$, where $D = x_R - x_L$, with

$$y(s \pm D) = y(s) \quad \text{for all } s \in [s_L, s_R],$$

in order to ensure one can find s_l and s_r with $s_L - D \leq s_l \leq s_0$ and $s_0 \leq s \leq s_R + D$ such that (A.3) holds.

(3) In the statement and proof of Lemmas 3–5 and Theorem 6 of [23] the value of a is $a = 4$, which yields a value for C_h , which is denoted \tilde{C}_h in this article in order to avoid confusion, of

$$\tilde{C}_h \stackrel{\text{def}}{=} \bar{C}_h[4] = \frac{\sqrt{4}-\sqrt{2}}{4\sqrt{2}\sqrt{4-1}} = \frac{\sqrt{2}-1}{4\sqrt{3}}. \tag{A.6}$$

(4) The conclusions of Theorem A.1 remain valid if the assumption the interface $z(s)$ is a simple closed curve is replaced by the assumption $z(s_L)$ and $z(s_R)$ lie on the boundary $\partial\Omega$ of the computational domain Ω , subject to the assumptions stated in the second paragraph of (5) on page 130. In addition, one must modify the proof of Lemma 5 in [23], since in this case there may not be a point s_l such that $\dot{x}^2(s_l) = 1/a$ or s_r such that $\dot{x}^2(s_r) = 1/a$; i.e., (A.3), which is the analog of equation (37) in [23], may not hold. See the comments concerning Lemma 4 in item (2) on pages 109–110 of [23] for the reason, if $z(s_L)$ and $z(s_R)$ lie on $\partial\Omega$, then this does not change the conclusions of Theorem A.1.

(5) If one chooses $a = 4.053301$, then the constant $\bar{C}_h[a]$ in (A.1) becomes

$$C_h \stackrel{\text{def}}{=} \bar{C}_h[a] = \frac{\sqrt{a} - \sqrt{2}}{4\sqrt{2}\sqrt{a-1}} = \frac{2}{33},$$

and the bound on the first derivative of the interface in (A.5a) becomes

$$\max_{x \in [x_l, x_r]} |g'(x)| \leq \sqrt{a-1} \approx \sqrt{3.053301} < 2. \quad (\text{A.7})$$

The value of $\sqrt{a-1}$ in (A.7) is a deliberate overestimate, the purpose of which is to simplify the bound on the expression in (56) that appears on the right-hand side of (57), and subsequent expressions that depend on the bound in (52).

(6) [Theorem A.1](#) ensures h is small enough that the interface can always be written as a single-valued function of one of the independent variables x or y in any 3×3 block centered on a cell containing a portion of the interface. This places an upper bound on C_h through (A.3) and (A.4). In addition, C_h is constrained both from above and below by the need to show inequalities of the form

$$\kappa_{\max} \geq \frac{g''(x)}{(\sqrt{a})^3} > \frac{C_h}{h}, \quad (\text{A.8})$$

hold in Equations (61), (69), and (78) in the proofs of Lemmas 11–13 of [23], respectively, where (A.5b) has been used to bound κ_{\max} from below by $g''/(\sqrt{a})^3$. Since in each of Equations (61), (69), and (78) of [23] the bound on g'' is of the form

$$g''(x) > \frac{\tilde{M}}{h} \quad \text{for all } x \in [x_{i-1}, x_{i+2}], \quad (\text{A.9})$$

equations (A.1), (A.8), and (A.9) lead to the requirement that $a > 2$ must satisfy the following inequality,

$$4\sqrt{2}\tilde{M}\sqrt{a-1} \geq (\sqrt{a})^4 - \sqrt{2}(\sqrt{a})^3. \quad (\text{A.10})$$

A careful study of this inequality will reveal the range of permissible values for a and hence, for $C_h = \bar{C}_h[a]$, is quite narrow.

References

- [1] I. Aleinov and E. G. Puckett, *Computing surface tension with high-order kernels*, Proceedings of the 6th International Symposium on Computational Fluid Dynamics (K. Oshima, ed.), 1995, pp. 6–13.
- [2] E. Aulisa, S. Manservigi, R. Scardovelli, and S. Zaleski, *A geometrical area-preserving volume-of-fluid advection method*, *J. Comput. Phys.* **192** (2003), no. 1, 355–364.
- [3] J. U. Brackbill, D. B. Kothe, and C. Zemach, *A continuum method for modeling surface tension*, *J. Comput. Phys.* **100** (1992), no. 2, 335–354. [MR 93c:76008](#)

- [4] A. J. Chorin, *Flame advection and propagation algorithms*, J. Comput. Phys. **35** (1980), no. 1, 1–11. [MR 81d:76061](#)
- [5] ———, *Curvature and solidification*, J. Comput. Phys. **57** (1985), no. 3, 472–490. [MR 86d:80001](#)
- [6] D. Gueyffier, J. Li, A. Nadim, R. Scardovelli, and S. Zaleski, *Volume-of-fluid interface tracking with smoothed surface stress methods for three-dimensional flow*, J. Comput. Phys. **152** (1999), no. 2, 423–456.
- [7] L. F. Henderson, P. Colella, and E. G. Puckett, *On the refraction of shock waves at a slow-fast gas interface*, J. Fluid Mech. **224** (1991), 1–27.
- [8] C. W. Hirt and B. D. Nichols, *Volume of fluid (VOF) method for the dynamics of free boundaries*, J. Comput. Phys. **39** (1981), 201–225.
- [9] R. M. Hurst, *Numerical approximations to the curvature and normal of a smooth interface using high-order kernels*, MS Thesis, University of California, Davis, 1995.
- [10] D. B. Kothe, J. R. Baumgardner, S. T. Bennion, J. H. Cerutti, B. J. Daly, K. S. Holian, E. M. Kober, S. J. Mosso, J. W. Painter, R. D. Smith, and M. D. Torrey, *PAGOSA: a massively-parallel, multi-material hydro-dynamics model for three-dimensional high-speed flow and high-rate deformation*, technical report LA-UR-92-4306, Los Alamos National Laboratory, 1992.
- [11] P. Lax and B. Wendroff, *Systems of conservation laws*, Comm. Pure Appl. Math. **13** (1960), 217–237. [MR 22 #11523](#)
- [12] R. J. LeVeque, *Numerical methods for conservation laws*, Lectures in Mathematics ETH Zürich, no. 72, Birkhäuser, Basel, 1990. [MR 91j:65142](#)
- [13] ———, *Finite volume methods for hyperbolic problems*, Cambridge Texts in Applied Mathematics, no. 31, Cambridge University Press, 2002. [MR 2003h:65001](#)
- [14] G. H. Miller and P. Colella, *A conservative three-dimensional Eulerian method for coupled solid-fluid shock capturing*, J. Comput. Phys. **183** (2002), no. 1, 26–82. [MR 2003j:76080](#)
- [15] G. H. Miller and E. G. Puckett, *Edge effects in molybdenum-encapsulated molten silicate shock wave targets*, J. Appl. Phys. **75** (1994), no. 3, 1426–1434.
- [16] ———, *A high-order Godunov method for multiple condensed phases*, J. Comput. Phys. **128** (1996), no. 1, 134–164.
- [17] B. D. Nichols, C. W. Hirt, and R. S. Hotchkiss, *SOLA-VOF: a solution algorithm for transient fluid flow with multiple free boundaries*, technical report LA-8355, Los Alamos National Laboratory, 1980.
- [18] W. F. Noh and P. R. Woodward, *SLIC (simple line interface calculation)*, technical report UCRL-77651, Lawrence Livermore National Laboratory, 1976.
- [19] ———, *SLIC (simple line interface calculation)*, Lecture Notes in Physics (A. I. van der Vooren and P. J. Zandbergen, eds.), no. 59, Springer, New York, 1976, pp. 330–340.
- [20] B. J. Parker and D. L. Youngs, *Two and three dimensional eulerian simulation of fluid flow with material interfaces*, technical report 01/92, UK Atomic Weapons Establishment, Aldermaston, Berkshire UK, 1992.
- [21] J. E. Pilliod, Jr. and E. G. Puckett, *Second-order accurate volume-of-fluid algorithms for tracking material interfaces*, J. Comput. Phys. **199** (2004), no. 2, 465–502. [MR 2005d:65145](#)
- [22] S. Popinet and S. Zaleski, *A front-tracking algorithm for the accurate representation of surface tension*, Int. J. Numer. Methods Fluids **30** (1999), no. 6, 775–793.
- [23] E. G. Puckett, *On the second-order accuracy of volume-of-fluid interface reconstruction algorithms: convergence in the max norm*, Commun. Appl. Math. Comput. Sci. **5** (2010), no. 1, 99–148. [MR 2011c:76001](#)

- [24] ———, *A volume-of-fluid interface reconstruction algorithm that is second-order accurate in the max norm*, Commun. Appl. Math. Comput. Sci. **5** (2010), no. 2, 199–220. MR 2012c:65130
- [25] E. G. Puckett and G. H. Miller, *The numerical computation of jetting impacts*, Proceedings of the 20th International Symposium on Shock Waves (New Jersey) (B. Sturtevant, J. E. Shepherd, and H. Hornung, eds.), vol. II, World Scientific, 1996, pp. 1467–1472.
- [26] Y. Renardy and M. Renardy, *PROST: a parabolic reconstruction of surface tension for the volume-of-fluid method*, J. Comput. Phys. **183** (2002), no. 2, 400–421. MR 2003k:76102
- [27] W. J. Rider and D. B. Kothe, *Reconstructing volume tracking*, J. Comput. Phys. **141** (1998), no. 2, 112–152. MR 99a:65200
- [28] R. Scardovelli and S. Zaleski, *Direct numerical simulation of free-surface and interfacial flow*, Annual Review of Fluid Mechanics, no. 31, Annual Reviews, Palo Alto, CA, 1999, pp. 567–603. MR 99n:76002
- [29] S. K. Stein and A. Barcellos, *Calculus and analytic geometry*, 5th ed., McGraw-Hill, 1992.
- [30] M. D. Torrey, L. D. Cloutman, R. C. Mjolsness, and C. W. Hirt, *NASA-VOF2D: a computer program for incompressible flows with free surfaces*, technical report LA-10612-MS, Los Alamos National Laboratory, 1985.
- [31] M. D. Torrey, R. C. Mjolsness, and L. R. Stein, *NASA-VOF3D: a three-dimensional computer program for incompressible flows with free surfaces*, technical report LA-11009-MS, Los Alamos National Laboratory, 1987.
- [32] M. W. Williams, D. B. Kothe, and E. G. Puckett, *Accuracy and convergence of continuum surface-tension models*, Fluid dynamics at interfaces (W. Shyy and R. Narayanan, eds.), Cambridge University Press, 1999, pp. 294–305.
- [33] D. L. Youngs, *Time-dependent multi-material flow with large fluid distortion*, Numerical methods for fluid dynamics (K. W. Morton and M. J. Baines, eds.), Institute of Mathematics and Its Applications, Academic Press, 1982, pp. 273–285.
- [34] ———, *Numerical simulation of turbulent mixing by Rayleigh–Taylor instability*, Proceedings of the Third Annual International Conference on Fronts, Interfaces, and Patterns (A. R. Bishop, L. J. Campbell, and P. J. Channell, eds.), North-Holland, 1983, Reprinted from Physica D, **12D** (1984), nos. 1–3, pp. 32–44.
- [35] ———, *An interface tracking method for a 3D Eulerian hydrodynamics code*, technical report AWRE/44/92/35, UK Atomic Weapons Research Establishment, 1987.

Received September 7, 2010. Revised November 13, 2012.

ELBRIDGE GERRY PUCKETT: egpuckett@ucdavis.edu

Department of Mathematics, University of California, Davis, One Shields Avenue, Davis, CA 95616, United States

Communications in Applied Mathematics and Computational Science

msp.org/camcos

EDITORS

MANAGING EDITOR

John B. Bell
Lawrence Berkeley National Laboratory, USA
jbbell@lbl.gov

BOARD OF EDITORS

Marsha Berger	New York University berger@cs.nyu.edu	Ahmed Ghoniem	Massachusetts Inst. of Technology, USA ghoniem@mit.edu
Alexandre Chorin	University of California, Berkeley, USA chorin@math.berkeley.edu	Raz Kupferman	The Hebrew University, Israel raz@math.huji.ac.il
Phil Colella	Lawrence Berkeley Nat. Lab., USA pcollella@lbl.gov	Randall J. LeVeque	University of Washington, USA rjl@amath.washington.edu
Peter Constantin	University of Chicago, USA const@cs.uchicago.edu	Mitchell Luskin	University of Minnesota, USA luskin@umn.edu
Maksymilian Dryja	Warsaw University, Poland maksymilian.dryja@acn.waw.pl	Yvon Maday	Université Pierre et Marie Curie, France maday@ann.jussieu.fr
M. Gregory Forest	University of North Carolina, USA forest@amath.unc.edu	James Sethian	University of California, Berkeley, USA sethian@math.berkeley.edu
Leslie Greengard	New York University, USA greengard@cims.nyu.edu	Juan Luis Vázquez	Universidad Autónoma de Madrid, Spain juanluis.vazquez@uam.es
Rupert Klein	Freie Universität Berlin, Germany rupert.klein@pik-potsdam.de	Alfio Quarteroni	Ecole Polytech. Féd. Lausanne, Switzerland alfio.quarteroni@epfl.ch
Nigel Goldenfeld	University of Illinois, USA nigel@uiuc.edu	Eitan Tadmor	University of Maryland, USA etadmor@cscamm.umd.edu
		Denis Talay	INRIA, France denis.talay@inria.fr

PRODUCTION

production@msp.org

Silvio Levy, Scientific Editor


See inside back cover or msp.org/camcos for submission instructions.

The subscription price for 2013 is US \$75/year for the electronic version, and \$105/year (+\$15, if shipping outside the US) for print and electronic. Subscriptions, requests for back issues from the last three years and changes of subscribers address should be sent to MSP.

Communications in Applied Mathematics and Computational Science (ISSN 2157-5452 electronic, 1559-3940 printed) at Mathematical Sciences Publishers, 798 Evans Hall #3840, c/o University of California, Berkeley, CA 94720-3840, is published continuously online. Periodical rate postage paid at Berkeley, CA 94704, and additional mailing offices.

CAMCoS peer review and production are managed by EditFLOW® from Mathematical Sciences Publishers.

PUBLISHED BY

 **mathematical sciences publishers**
nonprofit scientific publishing

<http://msp.org/>

© 2013 Mathematical Sciences Publishers

Communications in Applied Mathematics and Computational Science

vol. 8

no. 1

2013

- On the origin of divergence errors in MHD simulations and consequences for numerical schemes 1
FRIEDEMANN KEMM
- Renormalized reduced models for singular PDEs 39
PANOS STINIS
- Legendre spectral-collocation method for Volterra integral differential equations with nonvanishing delay 67
YANPING CHEN and ZHENDONG GU
- A cartesian grid embedded boundary method for the compressible Navier–Stokes equations 99
DANIEL T. GRAVES, PHILLIP COLELLA, DAVID MODIANO, JEFFREY JOHNSON, BJORN SJOGREEN and XINFENG GAO
- Second-order accuracy of volume-of-fluid interface reconstruction algorithms II: An improved constraint on the cell size 123
ELBRIDGE GERRY PUCKETT
- Computational models of material interfaces for the study of extracorporeal shock wave therapy 159
KIRSTEN FAGNAN, RANDALL J. LEVEQUE and THOMAS J. MATULA